DEVELOPMENT OF CIRCULATION CONTROL TECHNOLOGY FOR POWERED-LIFT STOL AIRCRAFT

Robert J. Englar
Advanced Flight Sciences Dept.
Lockheed-Georgia Company

SUMMARY

The flow-entraining capabilities of the Circulation Control Wing high-lift system have recently been employed to provide an even stronger STOL potential when synergistically combined with upper-surface-mounted engines. The resulting configurations generate very high supercirculation lift in addition to a vertical component of the pneumatically-deflected engine thrust. The present paper will discuss a series of small-scale wind tunnel tests and full-scale static thrust-deflection tests which provide a sufficient data base confirming the concepts, and show means of improving their STOL and cruise performance. These test results show thrust deflections of greater than 90^{o} produced pneumatically by non-moving aerodynamic surfaces, and the ability to maintain constant high lift while varying the propulsive force from high thrust recovery required for short takeoff to high drag generation required for short low-speed landings. Predicted takeoff and landing performance of a postulated aircraft employing the combined concepts will show their excellent STOL potential, and indicate the need for follow-on research.

INTRODUCTION

The Circulation Control (CC) airfoil has been under development since 1968 (see Ref. 1), with initial application intended for rotary wing vehicles. The underlying principle of operation is shown in Figure 1. Tangential blowing over a round or near-round trailing edge produces a balance between centrifugal force and sub-ambient pressure in the jet, causing the jet to follow the curved surface, generate very high negative pressures in that vicinity and thus strongly entrain the surrounding flowfield. The result is boundary layer entrainment, until the airfoil static pressures return to the inviscid distribution at relatively low momentum coefficient (C_{μ}). Beyond that, additional blowing yields supercirculation and resulting lift greater than that attainable by potential flow. Typical results of early airfoil tests shown in Figure 1 ($C_l > 6.5$ for $C_{\mu} < 0.25$) revealed a very strong potential for CC airfoils beyond application to rotary wing vehicles: fixed wing STOL aircraft using CC airfoils for high lift generation at very low power input. Experimental maximum lift exceeding that predicted by potential flow theory (Fig. 2) has been generated; the minimum blowing required for a given lift increment was far less than that required by traditional blown flaps of similar flap chord. The possibility of obtaining this low required momentum directly from compressor bleed ports of existing jet engines, and

thus supplying excellent STOL capability to high performance aircraft, led to a Navy program to develop the Circulation Control Wing (CCW). Numerous 2-D and 3-D experimental investigations (Refs. 2 and 3 are typical) at David Taylor Naval Ship R&D Center (DTNSRDC) lead to a proof-of-concept flight demonstration program on a Navy A-6 (Ref. 4). The resulting significant STOL capability was confirmed (Ref. 5 and 6), and led to a continuing program at DTNSRDC to develop an operational CCW system for Navy STOL aircraft. This Navy program and advanced developments in CCW configurations are discussed in Reference 7, while an additional flight test program on a propeller-driven CCW aircraft was conducted at West Virginia University (see Ref. 1 for data reports). These two programs very successfully confirmed the CCW potential for fixed wing STOL aircraft, with the capabilities either of operating at very low speeds from short fields (or aircraft carriers) or operating with greatly increased gross weights and lift-off/return payloads.

The flow-entrainment capabilities of the CC trailing edge have recently been proven to provide an even stronger STOL potential when synergistically combined with a powered-lift system such as upper surface blowing (USB). Existing USB aircraft (Ref. 8, for example) entrain and deflect engine exhaust by means of large mechanical flaps, and add both a vertical thrust component $C_T \sin(\alpha+\delta_j)$ and increased wing circulation lift (C_{L_Γ}) to the high-lift capability (Fig. 3). However, CCW alone has virtually no lift component due to vertical thrust recovery, and as Figure 3 shows, obtains most of its high lift due to supercirculation, C_{L_Γ}. Again, this is possible due to the very high suction peaks at the trailing edge and the resulting flow entrainment and negative pressures induced on the airfoil. From Fig. 3 analysis, it appeared quite logical that a synergistic configuration of the two configurations could produce an even more effective and versatile STOL aircraft. Thus, a combination of CCW and USB (Fig. 4) was patented and experimentally confirmed (Refs. 9 and 10) at DTNSRDC. The device exhibited not only very high lift capability but also the ability to interchange drag and thrust at a fixed lift value, and thus provide significant versatility for STOL aircraft on steep approaches or in wave-off maneuvers.

Recent static investigations conducted by DTNSRDC at NASA Ames on the Quiet Short-haul Research Aircraft (QSRA, Ref. 11) have confirmed full-scale static thrust turning greater than 90°. A second series of tests conducted on that aircraft developed improved CCW configurations that required even less blowing to provide usable thrust turning angles. In addition, recent work being conducted at Lockheed-Georgia Company has continued development of the CCW/USB data base and configurations, with specific attention being paid to the cruise mode. With the intention of reducing scrubbing losses due to USB exhaust immersing the wing upper surface in cruise, the Over-The-Wing (OTW) concept previously investigated by NASA (Ref. 12) has been re-evaluated and combined with CCW.

The present paper will elaborate on the above-mentioned developments of the circulation control wing concept integrated with various forms of powered-lift systems. It will provide further details on these recently conducted powered-lift research efforts, both model- and full-scale, and evaluate calculated STOL performance improvements when applied to an existing airframe/engine combination. Primary discussion will center on two recently

conducted series of investigations: a full-scale static development of CCW/USB on the NASA QSRA STOL aircraft, and smaller-scale model tests of CCW/USB and CCW/OTW. A summary of early experimental confirmation of the CCW/USB will precede these.

SYMBOLS

Values are given in SI and U.S. Customary Units, but measurements and calculations were made in the latter.

b_j	blowing jet slot span, cm (in.)
c	airfoil chord, cm (in.)
C_D	wing or aircraft drag coefficient (includes horizontal thrust component if a vectored-thrust configuration)
C_l, C_L	airfoil or wing (aircraft) lift coefficient
C_{L_Γ}	circulation lift coefficient
C_T	thrust coefficient, T/qS
C_μ	blowing momentum coefficient, $\dot{m}V_j/qS$
h, h_j	blowing jet slot height, cm (in.)
h_N	engine exhaust nozzle height, cm (in.)
M_j	blowing jet Mach number
M_{USB}	engine exhaust Mach number
$\dot{m}$	blowing jet mass efflux, kg/sec (slugs/sec)
N_1	engine fan speed, rpm
P_{CCW}, P_{T_d}	blowing plenum total pressure, N/m^2 (lb/ft^2)
q	freestream dynamic pressure, N/m^2 (lb/ft^2)
r	CC trailing edge radius, cm (in.)
S	wing area, m^2 (ft^2)
T	calibrated engine thrust, N(lb)
t/c	airfoil thickness-to-chord ratio
V_{APP}	velocity along approach flight path, m/sec (ft/sec)
V_j	blowing jet velocity, m/sec (ft/sec)
W_N	engine exhaust nozzle width, cm (in.)
α	angle of attack, deg.
α_{geo}	geometric angle of attack, uncorrected for tunnel interference effects, deg.
δ_F	flap deflection, deg.
δ_{USB}	Upper Surface Blowing flap deflection, deg.
θ, δ_j	jet or thrust deflection angle, deg. down from aft horizontal axis

SMALL-SCALE CONFIRMATION OF CCW/USB

The original concept of a CCW/USB combination occurred when the author was at DTNSRDC following the successful A-6/CCW flight test. An initial bench test was conducted on a semi-span CCW model joined with a turbofan engine simulator with a D-nozzle. Flow visualization indicated very large engine thrust deflection angles, and led to the mounting of the model on a tunnel balance frame for static confirmation. Figures 5 and 6 from Ref. 6 present

the results in terms of static jet turning angle (θ) as influenced by CCW blowing pressure and engine thrust level. Large turning angles of 165^{o} are confirmed, as is increased turning corresponding to increased CCW momentum. Two additional trends are also noted. Reduced turning occurs at higher thrust levels because of the additional energy in the engine exhaust that must be entrained by CCW. At constant higher thrust levels, peaks occur beyond which additional blowing yields reduced turning. This could very well be due to a characteristic previously noted for CCW alone (Ref. 13): higher blowing jet velocities, smaller turning radii and increased slot heights can reduce jet turning effectiveness. Figure 6 depicts the efficiency of this form of thrust deflection, with greater than 95 percent of the thrust and blowing momentum being recovered up through 55 degrees of thrust deflection. It also confirms a trend previously unseen in static USB data: thrust deflection of greater than 90^{o}, as well as the generation of both drag and thrust recovery from the same system.

Wind-on investigations, conducted on the same model in the DTNSRDC 8x10-ft. subsonic tunnel, confirm the lift augmentation possible with this system, in two modes of operation (Figure 7). These data, all taken at zero degrees geometric incidence, are for inboard blowing alone ("CC/USB only," solid symbols) and for CCW/USB combined with outboard blowing of a CCW segment ("CCW+CC/USB," open symbols). Inboard blowing alone confirms lift increase with both blowing and thrust increase, due to the increased exhaust deflection and entrained flow. However, the addition of outboard blowing of CCW yields additional lift at the same total C_{μ}. The drag polars confirm the versatility of the system, allowing at constant C_L the generation of either large drag values (for equilibrium approach) or large thrust values (for takeoff or climbout) merely by adjustment of thrust or blowing coefficient. Considerably more developmental work and configuration improvement was conducted at DTNSRDC on this concept, and is reported in detail in References 6, 9, 10, and 14.

LARGE-SCALE QSRA STATIC TESTS - PHASE I

An unknown in the above investigation was the effect of a real mixed-flow turbofan engine with hot exhaust, as well as the effects of scaling to full size. To address these issues, a joint DTNSRDC/NASA Ames full-scale static test was conducted, and is reported in detail in Reference 11. This Phase I test is summarized briefly here to provide a reference data base for the discussion which will follow on a second test series conducted to improve the CCW/USB configuration.

Figure 8 shows the NASA Quiet Short-Haul Research Aircraft (QSRA), a flight-proven Upper Surface Blowing powered-lift STOL aircraft, mounted on static thrust stands during the Phase I static tests conducted at NASA Ames Research Center. A CCW configuration can be seen mounted behind the inboard left engine only. Blowing was supplied using mass flow from standard aircraft ground starter carts, connected to the configuration as shown in Figure 9. The trailing edge radius was 3.62 percent of the average wing chord of the blown wing section, and the blowing slot height was set statically at 0.04 inch. Tufts in Figure 9 confirm the greater-than-90-degree jet turning

produced by the round trailing edge. These curving tufts contrast with a single tuft outboard of the blown section which plots the unaffected exhaust flow exiting aft nearly parallel to the wing upper surface. Static thrust turning resolved from the measured horizontal and vertical static forces is plotted in Figure 10, where trends very similar to the small-scale data of Figure 5 are noted. Actually, the apparently lower thrust turning angles of the full scale test are due solely to the fact that the mass flow output from the ground starter carts was insufficient to match the CCW blowing levels of Figure 5. A comparison between full-scale data and model data from Reference 14, adjusted to match the geometry of the QSRA arrangement, is shown in Figure 11. The agreement was quite good, considering some slight variation in parameters that were not exactly duplicated in the full-scale test (see Ref. 11). The conclusions drawn were that the full-scale hot configuration behaved in a very similar manner to the small-scale cold exhaust tests, jet deflections varied from 43 to 97 degrees at the higher blowing rate, and that additional full-scale jet deflections would result if greater CCW momentum were available. An additional item of interest is shown in Figure 12, where the Figure 10 data are nearly linearized when plotted against Mach number in the engine exhaust measured at the CCW jet slot location, instead of against calibrated engine thrust at the exhaust nozzle.

LARGE-SCALE QSRA STATIC TESTS - PHASE II

The above Phase I investigations revealed some refinements and improvements needed with the CCW/USB system, and suggested means to improve overall system performance and simplicity. Thus, a follow-on Phase II full-scale static investigation was conducted on the QSRA, the results of which will be discussed herein, and compared with the initial tests. Greater detail is found in Reference 15. The objectives of this Phase II series of tests included:

- refinement of CCW trailing edge shape and thickness to reduce cruise drag and determine if configurations other than large circular ones could improve performance,
- increase in blown system span and limitation of losses at the outboard end in order to further entrain more of the engine exhaust sheet,
- variation in blowing slot height to investigate additional entrainment, and
- increase in blowing slot momentum to investigate greater thrust deflection.

Design, Installation and Test Procedure

To investigate the above, two reduced-thickness CCW trailing edges of increased span and different structural arrangement were designed by DTNSRDC and constructed by Micro Craft Inc. of Tullahoma, Tennessee. These are shown in Figure 13 compared to the Phase I fully-circular large radius (r = .0362

chord) trailing edge. The 5-inch diameter 180-degree arc section was intended to reduce trailing edge thickness of the circular CCW device in blowing-off cruise by reducing the radius. The 10-inch diameter 90-degree arc section was intended to do the same, while maintaining the original larger radius of the Phase I configuration. This assumed that a maximum turning angle of 100 degrees from aft horizontal would be satisfactory from a STOL performance standpoint (if thrust reversing were not required). The span of the new configurations was increased to capture the larger spanwise spreading of the engine exhaust that had been exhibited in Phase I, and an outboard fence was installed to limit that spreading to the span of the blown section. Furthermore, variable slot height capability was provided. The five new configurations investigated during Phase II are further compared to the Phase I trailing edge below:

Phase	Config.	Dia., in.	Arc, deg.	Fence	Span, in.	Slot Ht, in.
I	--	10.0	260	Off	75.0	0.040-0.067
II	1	↓	90	↓	88.0	0.070
II	2	↓	↓	On	↓	↓
II	3	↓	↓	↓	↓	0.035
II	4	5.0	180	↓	↓	↓
II	5	↓	↓	↓	↓	0.070

Figures 14 and 15 show closeups of the 90-degree arc and the smaller-radius 180-degree circular arc as installed on the left inboard flap of the QSRA. Trailing edge thickness at the blowing slot location is the same for both, yet the radius of the 90-degree arc is twice as large. This eases the more difficult task for the CCW jet of entraining the high energy of the engine exhaust around a small radius, a phenomenon experienced in several aspects of previous CCW flow investigations (Ref. 13).

Figure 16 shows installation of the removable flow fence located 13" outboard of the separation line between the inboard and outboard mechanical USB flaps, which is where the Phase I trailing edge terminated. This figure also shows the blowing slot, pressure and temperature probes for the engine exhaust, support rod to restrict trailing edge upward deflection under load, and two of three air supply lines connected to the blowing plenum. These lines were connected to three conventional ground air-starter carts to supply the CCW trailing edge blowing; variation in blowing rate was simply by attaching or disconnecting another cart to the plenum. Slot height was pre-set at the values shown in the above chart, and then reset and measured when pressure and temperature had stabilized at each test condition. Since there were no flow meters in the starter cart system, the blowing mass flow ($\dot{m}_j$) and jet velocity (V_j) were calculated using the measured temperatures, pressures, and slot areas in the isentropic equations, just as they were in Phase I (see Ref. 11).

For relative comparison, the 90-degree arc configuration is shown on the QSRA in relation to the undeflected USB mechanical flap behind the outboard engine and the outboard double-slotted flap in Figure 17. On a production aircraft, the trailing edge of the CCW device would align with the conventional trailing edge, not be displaced aft of it as shown here. The

large size of the mechanical devices when deflected is hinted at by the size of the flap mounting brackets and fairings below the wing. A goal of this program was to eliminate the drag and complexity of these mechanisms as required for mechanical high-lift systems.

Results and Discussion, Phase II

Data from References 9, 10, 11 and 14 imply that CCW/USB thrust deflection is primarily a function of engine thrust level and CCW jet characteristics (mainly jet total pressure and momentum), while Reference 13 notes that CCW radius and slot height can strongly influence jet turning, especially at higher blowing pressures. Results of the Phase I test had confirmed some of the above relationships, as did the Phase II results. However, additional trends (such as effects of slot height and blowing span variations) were established during Phase II, and a number of performance improvements were seen.

Thrust Deflection and Recovery - Typical thrust deflection results from Phase II are shown in Figures 18 and 19, which represent two extremes in performance: the excellent turning produced by the larger radius 90-degree arc with a smaller slot height (Config. 3) compared to the considerably reduced turning of the smaller-radius 180-degree circular configuration with a larger slot height (Config. 5). At a typical blowing momentum per unit span of approximately 20 lb/ft at 75%N_1 engine power setting, the 90-degree arc produced 55 degrees of thrust deflection compared to about 37 degrees for the smaller radius 180-degree configuration. Note also for this latter configuration the much higher degree of resultant thrust loss per degree of turning at constant %N_1 (i.e., the more negative slopes of the lines marked constant N_1), a factor which could prove detrimental in climbout or go-around for a STOL aircraft.

An evaluation of the effect of reducing slot height can be made by comparison of Figure 20 with 19, both being for the small-radius 180-degree circular arc configuration. Here, for the same blowing momentum and power setting (say 20 lb/ft and 75%N_1), the smaller slot height yields greater turning compared to the larger slot height (47 degrees versus 37 degrees). This is because, at constant jet momentum, the reduced slot height's exit area must be balanced by increased jet velocity, which (up to certain higher limits on pressure ratio across the slot) produces greater flow entrainment and thrust deflection.

Whereas Figure 19 for the larger slot height confirms the additional thrust turning produced by additional momentum, that test objective was not met for the smaller slot heights. In Figures 18 and 20, the upper two sets of data (higher momenta) represent 2 and 3 ground start carts supplying air to the CCW. These should show the effect of a 50% increase in momentum, yet show little, if any, change in thrust turning. This was due to the fact that higher plenum pressure was required to produce a given momentum with a smaller exit area, and thus a limiting back pressure was reached (approximately 32-34 psig), beyond which the starter carts could produce no additional mass flow. Thus evaluation of the effect of jet momentum greater than about 20 lb/ft at

smaller slot height was not conducted and will require an alternative air supply source to complete.

For the above results, a resultant thrust vector was calculated for each test condition as the vector sum of static forces measured in the horizontal/vertical planes. This vector acted on the aircraft at the thrust deflection angle θ, measured positive downward from the aft horizontal. (No lateral forces are included due to lack of balance components in that direction.) As noted during Phase I (Ref. 11) and previous USB investigations, there is usually some loss in resultant thrust as jet turning increases, due to jet spreading, mixing and viscous losses. In Phase I, at maximum installed power, thrust recovery (resultant/installed thrust) varied from 98% with blowing off to 89% with maximum blowing momentum of 34.3 lb/ft. (Since blowing air came from the external ground starter carts, these recovery values do not include any thrust loss due to engine bleed, which would have to be considered in actual application). For comparison, Figures 21 and 22 present resultant thrust as functions of installed thrust, power setting and blowing rate for both the large- and small-radius CCW trailing edges and a 0.035-inch slot height. Thrust recovery for the 10-inch diameter 90^{o} arc (Fig. 21) is nearly the same as for the Phase I baseline configuration, but the smaller 5-inch circular arc shows considerably less recovery with blowing, down to about 83% at 20.7 lb/ft of blowing at maximum power setting. In general, for similar thrust deflection values, resultant thrust recovery is less with either smaller trailing edge radii or larger jet slot heights. These same trends were noted from the constant N_1 lines of Figures 18, 19, and 20. These trends produce mixed implications in STOL operation, where thrust loss is advantageous on approach along steep glide slopes, but is definitely detrimental on takeoff, climbout or waveoffs (go-arounds).

A typical resolution of measured horizontal and vertical forces and their variation with blowing is shown in Figure 23. Here the versatility of the CCW/USB concept is evident: constant vertical force may be maintained while horizontal force is varied pneumatically. Conversely, constant horizontal force may be held while lift is increased by blowing, again without incidence or mechanical changes. The payoff for STOL aircraft, when the aerodynamic forces are added to these static values, will become more evident in a later section on STOL performance.

Configuration Comparison- A comparison of the effectiveness of the full-scale configurations tested in Phase II with the Phase I baseline is shown in Figures 24 and 25 for values of constant resultant thrust. Resultant thrust levels of 2500 and 5000 pounds represent approximately half- and full-power settings of the engine as installed in this test setup. In Figure 24, blowing momentum is plotted per unit span to offset the effect of additional momentum corresponding to increased slot length. Blowing off, the geometric camber of the Phase I circular configuration increased thrust deflection by 10-11 degrees over the Phase II configurations as well as the basic USB undeflected flap. The 90-degree arc (configuration 3) produced only 1 to 2 degrees incremental turning with blowing off. Large thrust deflection in cruise could prove detrimental because of horizontal thrust loss.

With blowing applied, a number of performance increases were noted. The increased span and endplate of the Phase II 10-in.-diameter configuration 3 nearly doubled the incremental thrust turning due to blowing when compared to the same radius configuration of Phase I. The flow fence alone produced a 2- to 4-degree increase in thrust deflection (Configuration 2 vs. 1). A doubling of the trailing edge radius (Configuration 3 vs. 4) increased thrust turning by 8 to 10 deg, but produced no difference in the blowing-off thrust deflection due to geometric camber. Reducing the slot height by 50 percent (Configuration 3 vs. 2, or 4 vs. 5) added 8 to 15 deg of thrust deflection at the same momentum. These data extend to CCW/USB the Reference 13 findings that flow entrainment over curved surfaces with blowing becomes more difficult with smaller radii, larger slot heights, and higher entrained flow velocity (i.e., greater engine thrust).

Figure 25 supplies useful design data for STOL application of this system, as it provides blowing momentum required for a given thrust deflection as a percentage of installed engine thrust. Since turbofan engine thrust loss can become appreciable when increased bleed is taken from the core, it is desirable to keep the bleed momentum as low as possible for takeoff and climbout. From this viewpoint, it is seen that for a typical thrust deflection of 40 degrees, the 90-degree arc (Config. 3) requires bleed momentum equal to 1.7 percent of the installed thrust, at full power setting. The Phase I configuration required about 4.6 percent to obtain the same turning, while the smaller diameter 180^{o} arc with larger slot height does not appear able to reach that value at all, probably due to the high exhaust energy level and small turning radius. For STOL approaches, where large thrust deflections are desired, the 90-degree arc at half-power setting can produce 60 degrees deflection using 5% of engine thrust as blowing momentum, a value which might typically be bled from the core of the engine; higher values become progressively more difficult to obtain. At the same half-power setting and 5% bleed, the smaller radius 180-degree arc produced 53 degrees jet deflection while the Phase I arc produced 48 degrees. The smaller radius was not as greatly affected by high exhaust velocity at this reduced power setting.

The above results indicate that the most effective trailing edge configuration from a thrust-turning standpoint was found to be the 10-in.-diameter 90-degree circular arc. It provided the same thrust turning as the other configurations while using considerably less momentum, or produced greater thrust turning at the same momentum. Exact comparison with the 10-in.-diameter circular cylinder of Phase I was not possible due to span and other geometry differences, but indications were that additional physical arc greater than 90 degrees performed little useful function. For the range of blowing investigated, a summary performance comparison can best be seen in the following chart of increase in jet deflection due to blowing:

Configuration	$T_{resultant}$, lb.	$\Delta\theta$, deg.
Baseline, Ph.I	2500	26.2
Config. 3, Ph. II	2500	46.0
Baseline, Ph. I	5000	13.8
Config. 3, Ph. II	5000	29.5

Excluding the effects of slightly smaller slot height and better blowing slot lip alignment of the 90-degree circular arc with h_j = 0.035 inch and larger span, that configuration roughly doubled the jet deflection due to blowing of the baseline Phase I configuration. It thus appears that one of the most effective means of increasing jet deflection is to ensure that the entire spread exhaust from the USB engine is captured by the CCW jet. With that provision, very effective pneumatic thrust turning can thus be produced by a much thinner partial arc trailing edge shape, which produces almost no thrust loss in cruise due to camber-induced deflection, and should have considerably reduced base drag. Thus, the performance improvements sought by the Phase II investigation were achieved by configuration improvement, and the new configurations developed should yield not only improved STOL performance, but increased cruise efficiency as well.

STOL APPLICATION AND PREDICTED PERFORMANCE

In order to investigate possible payoffs of the above thrust-vectoring and lift-augmenting technology, a STOL aircraft was postulated, employing the combination of CCW outboard and CCW/USB inboard (Ref. 9). The basic airframe chosen was the Lockheed S-3A Viking, with its existing TF-34 high-bypass turbofan engines retained but re-mounted on the wing in the USB arrangement shown in Figure 26. As the intended mission for this proposed aircraft was STOL operation from small-deck carriers, the original S-3A aspect ratio of 7.73 was reduced to 6.0 to allow flight deck clearance. The CCW/USB data of Figure 7 was used, but adjusted (see Ref. 9) to account for the aspect ratio difference and blowing-off characteristics of the basic S-3. The lift curves of Figure 27 resulted. (The standard S-3A still retains its 7.73 aspect ratio). Since no engine bleed data or thrust turning results were available for this configuration, it was assumed that a C_μ of 0.10 would be obtainable (perhaps from fan rather than core bleed) and that a thrust deflection angle of 38^o was attainable at all thrust settings. A round trailing edge CCW/USB configuration similar to that of the above Phase I test was assumed. In light of the Phase II tests results above, all of these conditions seem to be conservative, and thus the following performance predictions should represent at least a lower level of attainable performance for this type of configuration.

Takeoff Performance

All STOL performance discussed below is based on sea level tropical day ($90^{o}F$) conditions with standard S-3/TF-34 maximum two-engine installed thrust of 13,020 lb total, which include losses due to thrust droop, ram drag at 60 kts, and bleed. Since high thrust/weight ratio can be an important benefit in achieving short takeoff ground rolls, it is important to note that for the S-3A takeoff gross weight range (35,000-40,000 lb), the effective thrust/weight ratio is a relatively low 0.33 - 0.38, as Fig. 28 shows.

For this weight range, conventional S-3A (CTOL) lift-off speeds of 115 knots can be reduced to 60-65 knots by CCW/USB. The implications on reduced requirements for catapult equipment (if, in fact, any is required at all) are significant. The resulting non-catapulted takeoff distances are compared in Fig. 28 for wind-over-deck (WOD) velocities of 0 and 20 knots. Here, the takeoff procedure for the proposed aircraft is to accelerate at maximum thrust (bleed off and no thrust deflection) until the rotation speed is reached. At rotation, blowing is initiated and instantaneous thrust deflection and lift augmentation occur. This procedure was successfully and comfortably used by Grumman test pilots with the A-6/CCW (Ref. 5). For a 20 knot WOD, conventional S-3 takeoff rolls of 1,175 - 1,650 ft will be reduced to 200 - 325 ft. Takeoff distances of 450 - 650 ft are possible if no wind over deck is available.

Landing Performance

Using the conservative assumptions of only 38^{o} thrust deflection and 0.10 blowing coefficient, Fig. 29 compares equilibrium approach speeds at an incidence of 9^{o} or 10^{o} on a 4^{o} glide slope. Since no flare is used in Navy approaches, this glide slope is constant and forces must be in equilibrium along that flight path to avoid acceleration down it. This requires additional drag generation for USB aircraft since high lift is achieved at high thrust settings which normally result in high thrust recovery. This thrust recovery is offset for the CCW + CCW/USB aircraft by the induced drag generated by CCW. Thus all approaches are made along the $C_D = 0$ axis (see Fig. 7) but at the appropriate approach incidence of 10^{o}. For a landing weight of 30,000 - 35,000 lbs, the approach speed is reduced from 95 to 55 knots by the CCW + CCW/USB. For a fixed bleed rate from the engines, available C_μ will not remain constant, but will increase as weight and associated speed decrease. Thus Figure 29 also shows approach speeds at a fixed bleed momentum of 1130 lbs. total, which is felt to be attainable for this configuration. Approach speeds below 50 kts are now possible. These very low approach speeds plus any wind over deck will reduce touchdown speeds, kinetic energy to be dissipated, and landing ground rolls by as much as 70 percent. They also imply the capability for an improved steeper glide slope to minimize flight through carrier-induced turbulence, increased pilot visibility from approach at lower incidence, and increased pilot reaction time due to lower closure rates, all of which contribute to safer carrier operations and thus reduced accident rates.

The above STOL performance predictions indicate significant potential for aircraft operation from small air-capable ships, plus a number of operational

benefits for land-based aircraft as well, resulting from the incorporation of CCW/USB.

SMALL-SCALE ADVANCED CONFIGURATION DEVELOPMENT

While the above developments primarily addressed the high-lift pneumatic STOL configurations, an obvious outgrowth which cannot be overlooked is the associated cruise performance. The immersion of the wing upper surface and trailing edge in the engine exhaust, which is responsible for the thrust-induced lift generated by the CCW/USB configuration, also produces thrust loss due to exhaust scrubbing on these surfaces in the cruise mode. With the intention of reducing these losses without detriment to STOL thrust deflection, the Over-the-Wing (OTW) concept previously investigated by NASA (References 12 and 16) is being re-evaluated and refined at the Lockheed-Georgia Company. As shown schematically in Figure 30, the USB engine is relocated in the OTW configuration onto a pylon above the wing. Reference 16 confirms that this will eliminate the scrubbing drag and, in fact, if the undeflected exhaust nozzle is properly located, can reduce the induced drag in cruise by inducing an upwash on the wing. Recent research conducted at Lockheed-Georgia has focused on developing the high-lift OTW configuration by replacing the mechanical flap system with CCW configurations, and increasing the system's ability to deflect OTW thrust by improving the CCW turning surface geometry.

A generic powered-lift model has been used in these investigations; it is shown in Fig. 31 installed in the Lockheed 30x43-inch Model Test Facility, spanning the 30-inch width of the tunnel in a "quasi 2-D" mode with a chord-to-tunnel height ratio of 5.4. Force data from the floor balance, as well as pressure data from model static taps and a wake rake, were recorded. The model wing could be retracted through the tunnel floor to allow variation in aspect ratio. The same model is shown in Figure 32 as a semi-span aspect ratio 5.5 configuration. The OTW engine as shown was mounted on a wing pylon and employed a nozzle hood to deflect thrust onto the wing surface instead of the mechanical exhaust nozzle shown in the lower portion of Figure 30. For system comparison, the engine was also located on the wing surface and a D-nozzle installed to represent a USB configuration.

Test Results and Discussion

Figure 33 compares lift results for USB and OTW engine arrangements using both CCW and a single-slotted flap to entrain and deflect the thrust. In this "quasi 2-D" mode, as well as in the AR = 5.5 semi-span mode, the wing reference area is considerably larger than that affected by the engine thrust deflection, and thus the thrust coefficients evaluated (C_T = T/qS) are typically lower than would be expected of a STOL aircraft with proportional sizing of wing and engine. For the same trailing edge type, the following trends were noted:

- With the single-slotted mechanical flap, OTW yields greater induced lift and thrust recovery than does USB.

- With moderate thrust and blowing, there is relatively little difference between OTW and USB when combined with CCW. This confirms that CCW is able to entrain the thrust from the OTW engine nacelle which is further above the turning surface than it is for USB. It does however require a nozzle hood device, but the implication is that the two concepts are then equivalent in STOL while OTW should demonstrate reduced thrust loss in cruise.

Cross-plane velocity vectors obtained from 7-hole-probe rake surveys of the wing wake show the effect of the trailing edge high lift device on OTW performance in Figure 34. Clearly, the CCW blowing spreads, deflects and diffuses the exhaust plume, thus enhancing the lift by as much as 75 percent over the OTW/mechanical flap at low incidence, as shown in Figure 33. The engine downwash directly behind the wing is greatly reduced, thus reducing the possibilities of tail stall due to downwash immersion, ground fountain effects in STOL, and large nose-down pitching moments.

In order to generate additional blowing-off lift due to geometric camber, to provide a control device on thrust deflection with blowing, and to provide increased thrust recovery, the round CCW trailing edge used above was converted to a CCW flaplet by addition of an 11.4% plain flap, as shown in Figure 35. This flaplet had straight upper and lower surfaces making 14-degree angles with the chord line, and pivoted about its center on the chordline directly below the blowing slot. The radius exposed as the flap deflected was the same as the original CCW round trailing edge (.031c). A previous series of quasi 2-D investigations at various flaplet angles led to the choice of this 60-degree flap deflection, with the emphasis being on lift augmentation combined with engine and CCW jet thrust recovery.

Resulting lift generated at two CCW blowing levels and two engine thrust levels, as well as data for the plain CCW wing without the engine installed, are shown in Figure 35. An interesting comparison at these lower thrust levels shows that much greater lift augmentation per unit momentum input results from CCW blowing than from thrust deflection. As an example, at C_μ = 0.46, C_L is 2.8 to 3.0 higher than for C_μ = 0, while for C_T = 0.46, C_L is only 0.25 to 0.40 more than for C_T = 0 ("No engine").

The above data were used to extrapolate the CCW/OTW drag polars in Figure 36 to a typical C_T of 2.0. At this thrust level, and over a typical CCW blowing range of C_μ = 0 to 0.4, almost the entire envelope of drag polars lies in the negative drag (positive thrust recovery) region. This is quite desirable for short takeoff, climbout or waveoff, but it can produce a serious problem during a STOL approach: the aircraft cannot generate enough drag to offset the higher engine power level, and thus equilibrium slow-speed approach down a steep glide slope becomes quite difficult, if not impossible.

To generate this required drag, a means of increasing thrust deflection to higher angles is necessary such that little thrust is recovered under approach conditions. The round CCW trailing edge provides a means to do this, as shown by the data from Reference 14 plotted in Figures 35 and 36. As an example, at a C_T = 1.2 and C_L = 3.5, drag coefficient is converted from -0.50 for the 60-degree flaplet to +0.75 for the round CCW.

Although the aspect ratio (AR=4) and the engine arrangement (CCW/USB) of Reference 14 are not exactly comparable with the current model, the similar C_T and C_μ values serve to illustrate the trend: namely, additional turning produced by the round CCW trailing edge can reduce the thrust recovery and increase total drag. Thus, the desired compromise configuration to provide excellent operation in all regions of the STOL flight envelope is one which generates high lift augmentation in all configurations, but at the same time simply and effectively allows high thrust recovery on takeoff and climbout and high drag generation on approach. The further constraint of an efficient clean aircraft cruise configuration is, of course, mandatory.

To pursue these objectives, the CCW Dual Radius configuration developed in References 7 and 17 was combined with OTW. Here the flat upper surface of the short-chord flaplet of Figure 35 was converted to a large secondary radius to yield an additional 36 degrees of turning surface for the CCW jet and engine thrust. Figure 37 shows resulting lift and drag. The dual radius CCW flap alone, when deflected 90^o, generates similar lift and much higher drag than the 60^o flaplet OTW configuration at $C_T = 3.0$. However, when combined with OTW, the dual radius CCW flap increases C_L by as much as 2.5, yet allows thrust to vary from $C_D = -2.0$ to $+ 1.2$ merely by varying C_μ and resulting thrust deflection. Furthermore, tests of the undeflected dual radius CCW alone in a cruise configuration showed drag reduction of 14 percent compared to the undeflected flaplet and 40 percent that of the round CCW ($r = .031c$).

CONCLUSIONS

The above static full-scale and wind-on model-scale results have provided valuable confirmation that CCW can be effectively combined with an above-wing-mounted (USB or OTW) engine system to yield pneumatic thrust deflection and associated lift augmentation. The more important conclusions are:

- CCW flow entrainment can yield pneumatic thrust deflections of 90 degrees or greater from USB-mounted engines, and resulting model-scale maximum lift coefficients of 8-9.

- Improved CCW/USB configurations employing thinner, less-cambered partial arc trailing edges with smaller slot heights and increased blowing spans have yielded improved STOL potential.

- Pneumatic control of lift augmentation and horizontal thrust recovery increases STOL versatility, allowing simple conversion from high drag to high thrust recovery while maintaining a constant lift force. Variation of the combined aerodynamic/propulsive forces is thus seen to be possible without change in angle of attack or deflection/retraction of any external moving parts.

- Advanced versions of CCW and pneumatic thrust deflection can simplify powered-lift systems and improve cruise efficiency by eliminating viscous scrubbing losses. CCW/OTW configurations offer STOL performance similar to CCW/USB, as well as improvements in cruise drag

and efficiency. Both systems make possible few- or no-moving-part powered-lift systems capable of excellent STOL performance.

Small- and large-scale wind tunnel investigations are continuing at Lockheed-Georgia to further develop this technology for useful STOL application. The ultimate test, however, will be a full-scale powered-lift flight program, such as that recommended by Reference 18, where it is proposed to convert the QSRA to a CCW/USB configuration by relatively simple modification to the flaps. This will allow a logical continuation of the above static ground tests and in-flight verification of the indicated STOL potential of these pneumatic thrust-deflecting lift-augmenting concepts.

REFERENCES

1. Englar, R. J. and C. A. Applegate, "Circulation Control - A Bibliography of DTNSRDC Research and Selected Outside References (Jan 1969 through Dec 1983)" DTNSRDC Report 84/052, Sept 1984.

2. Englar, R.J., "Subsonic Two-Dimensional Wind Tunnel Investigations of the High Lift Capability of Circulation Control Wing Sections," DTNSRDC Report ASED-274, April 1975.

3. Englar, R.J., "Development of the A-6/Circulation Control Wing Flight Demonstrator Configuration," DTNSRDC Report ASED-79/01, Jan 1979.

4. Englar, R.J., R. A. Hemmerly, W. H. Moore, V. Seredinsky, ..G. Valckenaere, and J.A. Jackson, "Design of the Circulation Control Wing STOL Demonstrator Aircraft," AIAA Paper No. 79-1842 presented at the AIAA Aircraft Systems and Technology Meeting, New York, Aug 1979. AIAA Journal of Aircraft, Jan 1981, pp. 51-58.

5. Pugliese, A. J. and R. J. Englar, "Flight Testing the Circulation Control Wing," AIAA Paper No. 79-1791 presented at the AIAA Aircraft Systems and Technology Meeting, New York, Aug 1979.

6. Nichols, J.H., Jr. and R.J. Englar, "Advanced Circulation Control Wing System for Navy STOL Aircraft," AIAA Paper No. 80-1825 presented at the AIAA Aircraft Systems Meeting, Anaheim, California, Aug 1980. AIAA Journal of Aircraft, Dec. 1981, pp. 1044 - 1050.

7. Nichols, J. H., Jr. and M. J. Harris, "Fixed Wing CCW Aerodynamics — A Review," NASA Ames Circulation Control Workshop, NASA CP-2432, 1986 (Paper 21).

8. Sleeman, W.C. and W.C. Hohlweg, "Low-Speed Wing-Tunnel Investigation of a Four-Engine Upper Surface Blowing Model Having a Swept Wing and Rectangular and D-Shaped Exhaust Nozzles," NASA TN D-8061, Dec 1975.

9. Nichols, J. H., Jr., R.J. Englar, M.J. Harris, and G.G. Huson, "Experimental Development of an Advanced Circulation Control Wing System for Navy STOL Aircraft," AIAA Paper No. 81-0151 presented at the AIAA 19th Aerospace Sciences Meeting, St. Louis, Missouri, Jan 1981.

10. Harris, M. J., J.H. Nichols, Jr., R.J. Englar, and G.G. Huson, "Development of the Circulation Control Wing/Upper Surface Blowing Powered-Lift System for STOL Aircraft," Paper No. ICAS-82-6.5.1 presented at the 13th Congress of ICAS/AIAA Aircraft Systems and Technology Conference, Seattle, Aug. 1982.

11. Eppel, J. C., M.D. Shovlin, D.N. Jaynes, R.J. Englar, and J.H. Nichols, Jr., "Static Investigation of the Circulation Control Wing/Upper Surface Blowing Concept Applied to the Quiet Short-Haul Research Aircraft," NASA Technical Memo 84232, July 1982.

12. Coe, P. L., Jr., and Fournier, P. G., "Application of Powered Lift Concepts for Improved Cruise Efficiency of Long-Range Aircraft." NASA SP-406, pp. 89-101.

13. Englar, R. J., "Experimental Investigation of the High Velocity Coanda Wall Jet Applied to Bluff Trailing Edge Circulation Control Airfoils," DTNSRDC Report 4708, Sept 1975.

14. Harris, M. J., "Investigation of the Circulation Control Wing/Upper Surface Blowing High Lift System on a Low Aspect Ratio Semispan Model," DTNSRDC Report ASED-81/10, May 1981.

15. Englar, R.J., J.H. Nichols, Jr., M.J. Harris, J.C. Eppel, and M.D. Shovlin, "Development of Pneumatic Thrust Deflecting Powered-Lift Systems," AIAA Paper No. 86-0476, presented at AIAA 24th Aerospace Sciences Meeting, Reno, NV, Jan 1986.

16. Bower, R. E., "Opportunities for Aerodynamic-Drag Reduction." NASA SP-372, 1975, pp. 323-352.

17. Englar, R. J. and G. G. Huson, "Development of Advanced Circulation Control Wing High Lift Airfoils," AIAA Paper No. 83-1847 presented at the AIAA Applied Aerodynamics Conference, Danvers, MA, July 1983; AIAA Journal of Aircraft, July 1984, pp. 476-483.

18. Riddle, D. W. and J. C. Eppel, "A Potential Flight Evaluation of a USB/CCW Concept on the Quiet Short-Haul Research Aircraft," NASA Ames Circulation Control Workshop, NASA CP-2432, 1986 (Paper 23).

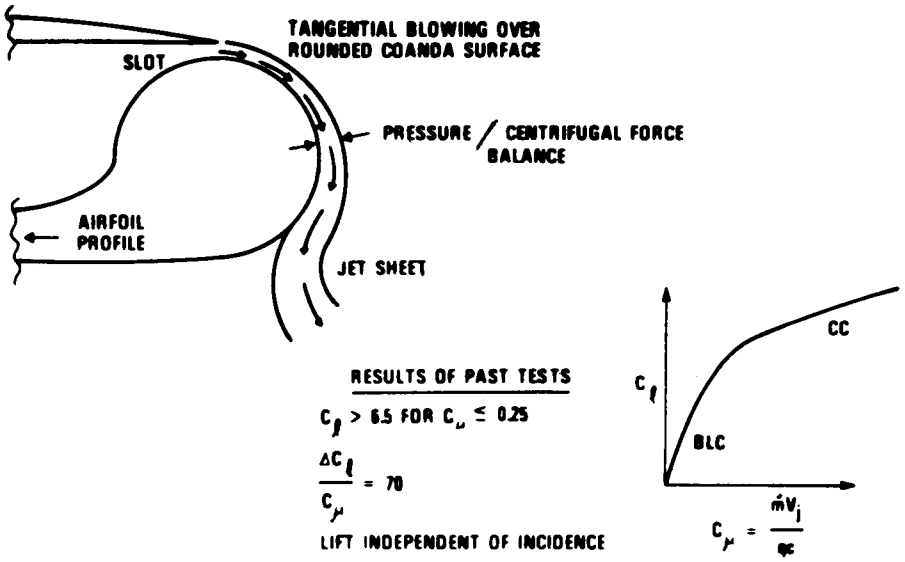

Figure 1. Basic Circulation Control Aerodynamics

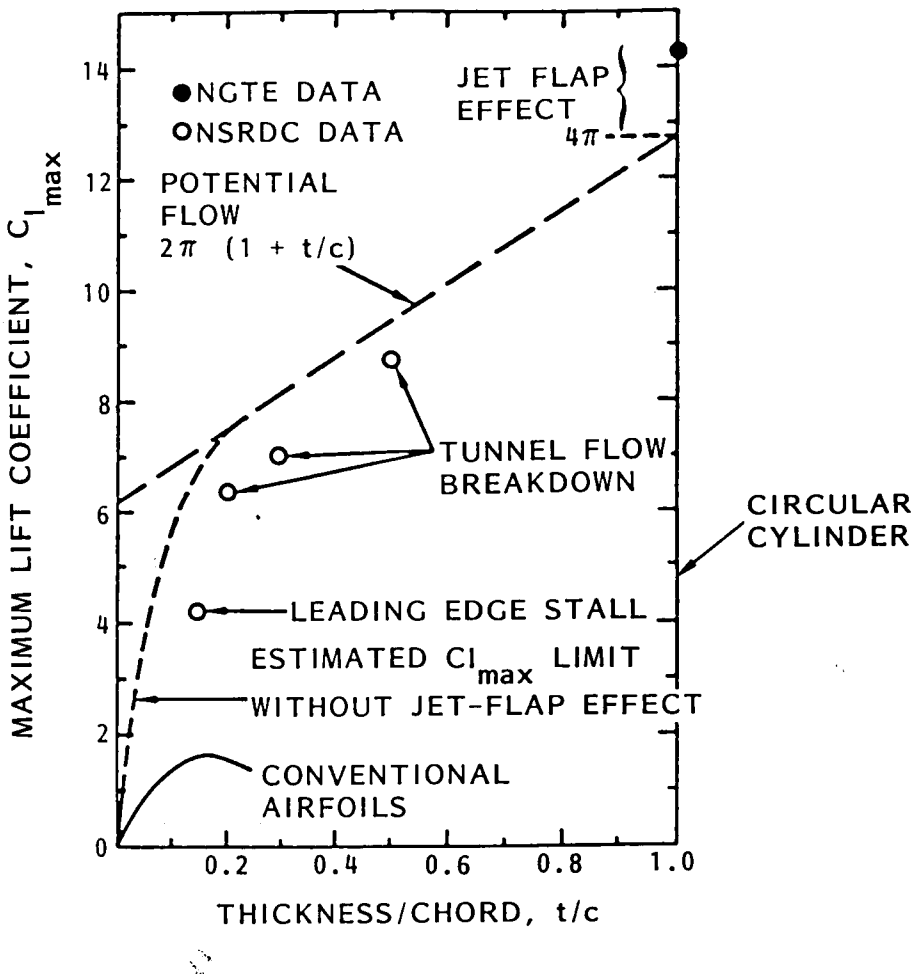

Figure 2. CC Airfoil Maximum Lift Coefficients

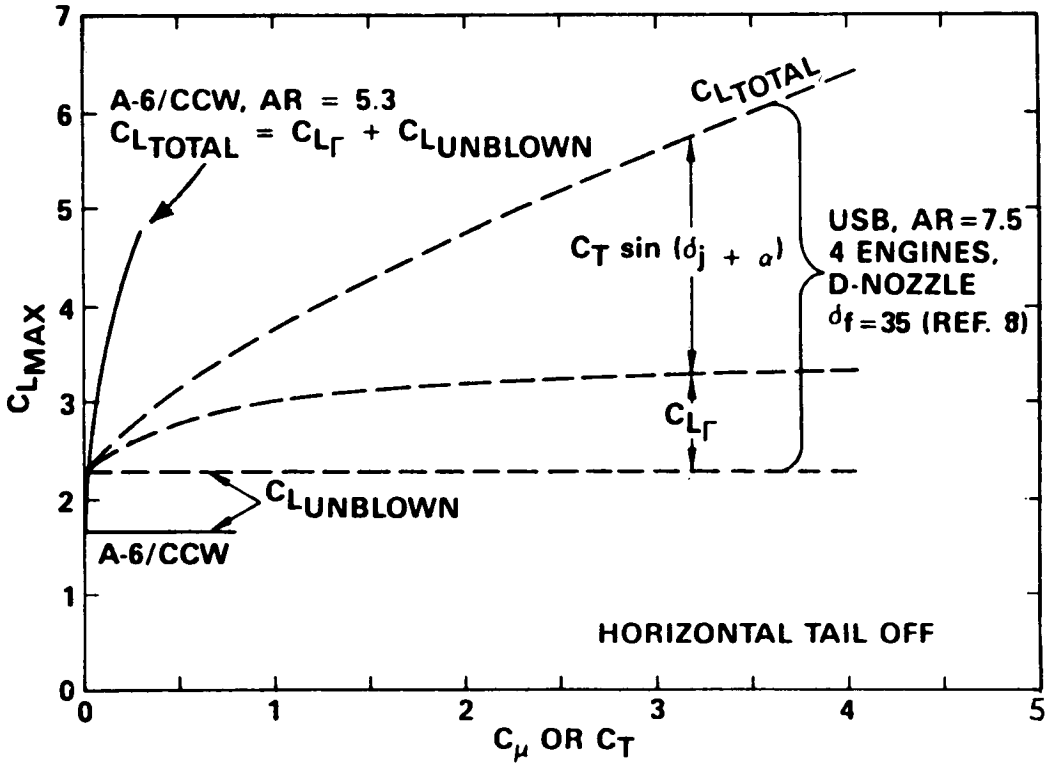

Figure 3. Maximum Lift for Typical CCW and USB Aircraft

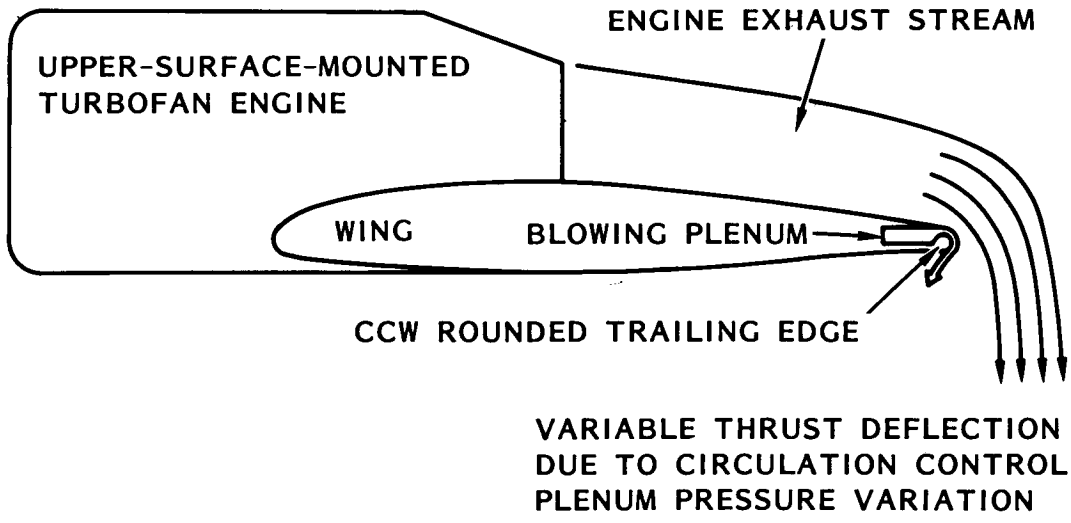

Figure 4. Circulation Control Wing/Upper Surface Blowing Powered-Lift System

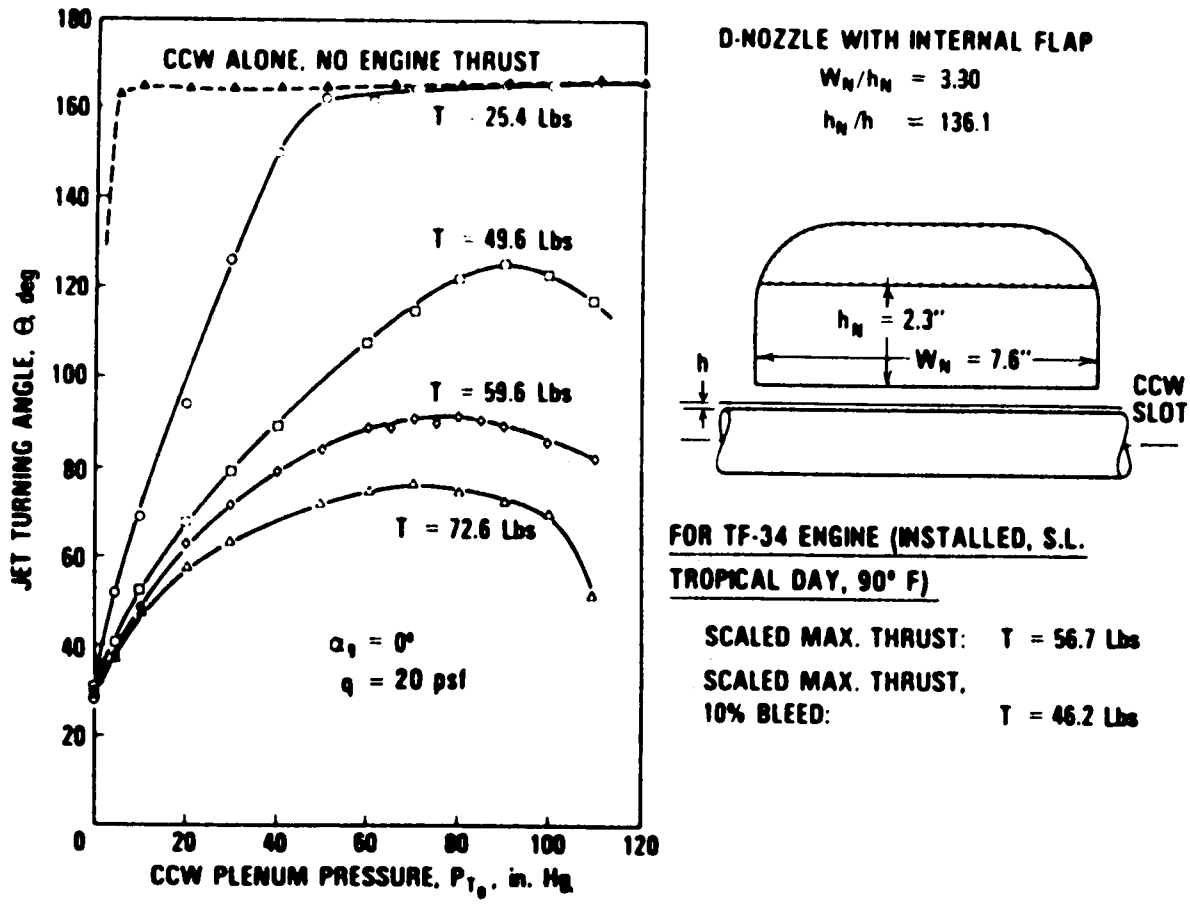

Figure 5. CCW/USB Static Thrust Turning, AR = 4 Semi-Span Model

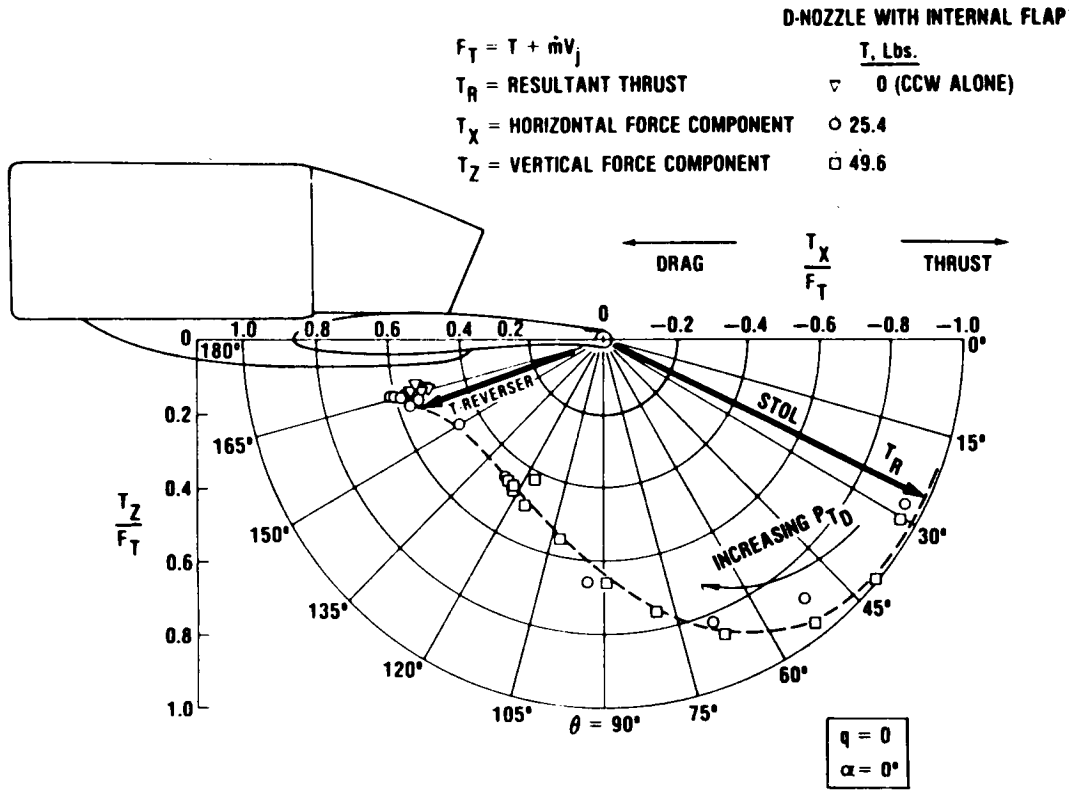

Figure 6. CCW/USB Static Turning Angle and Thrust Recovery Efficiency, AR = 4 Model

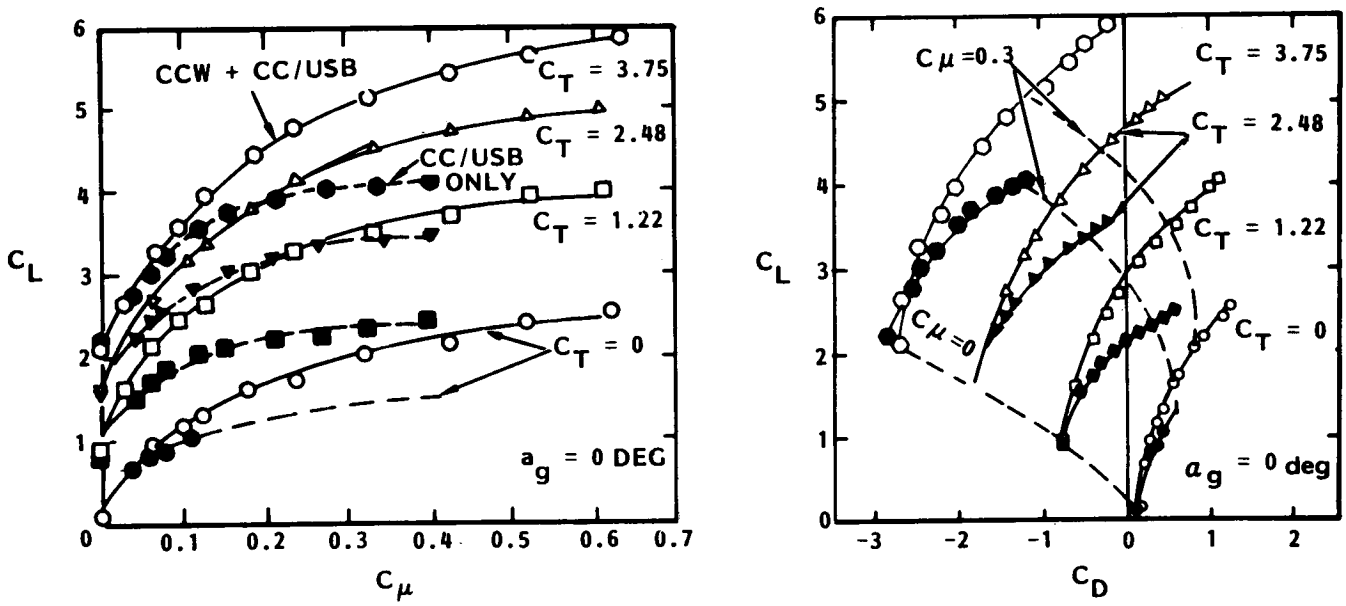

Figure 7. Effect of Blowing and Thrust Deflection on Lift and Drag (Ref. 14 Semi-Span Model)

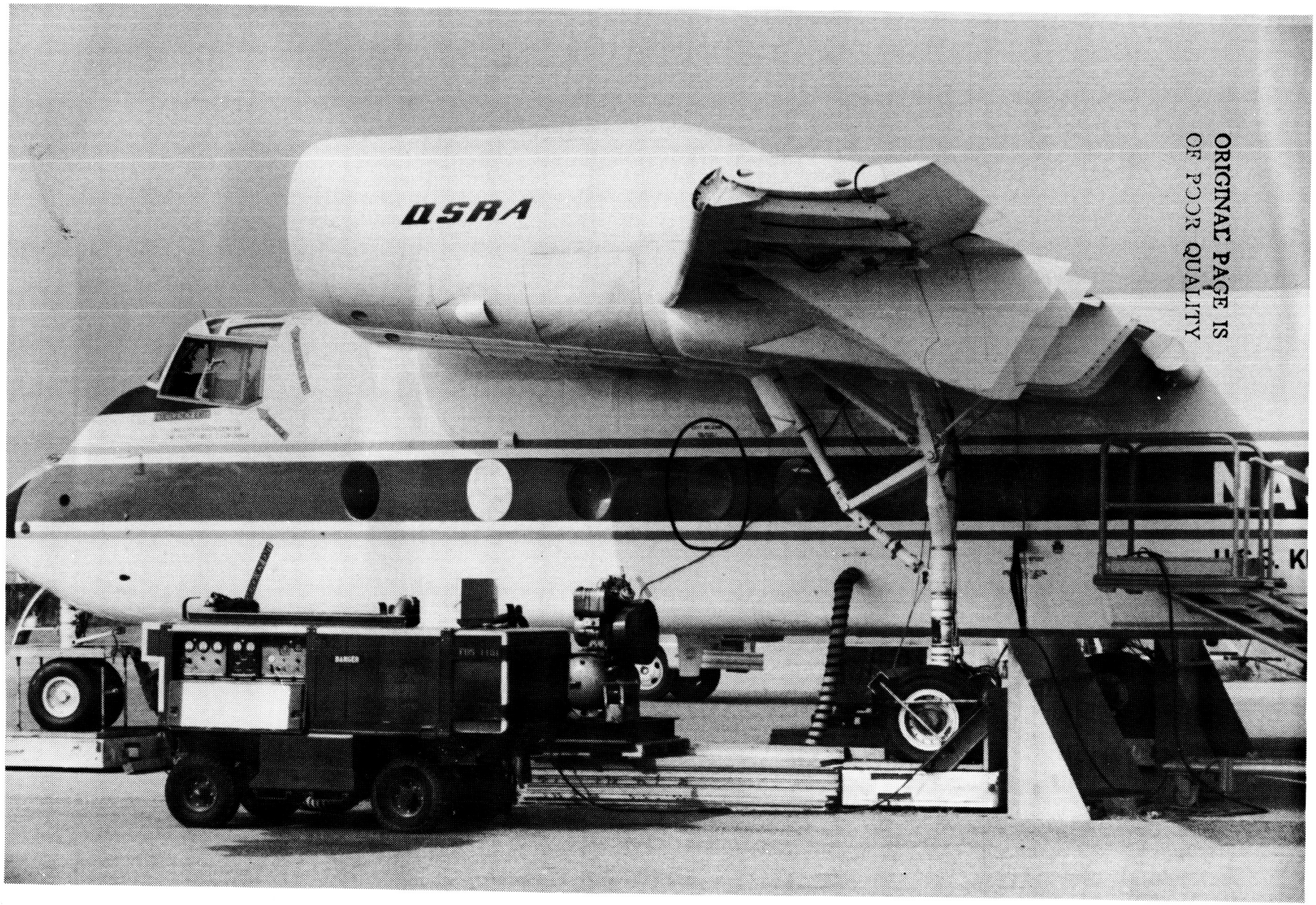

Figure 8. QSRA CCW/USB Phase I Static Test Setup

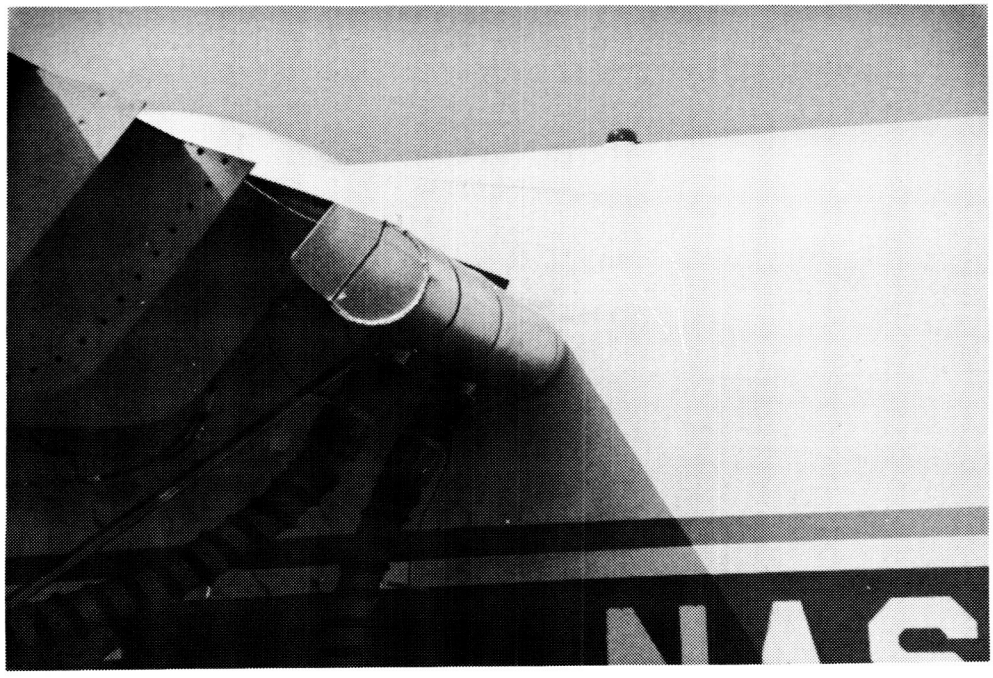

Figure 9. Blowing-On Static Thrust Deflection at the CCW Trailing Edge, Phase I

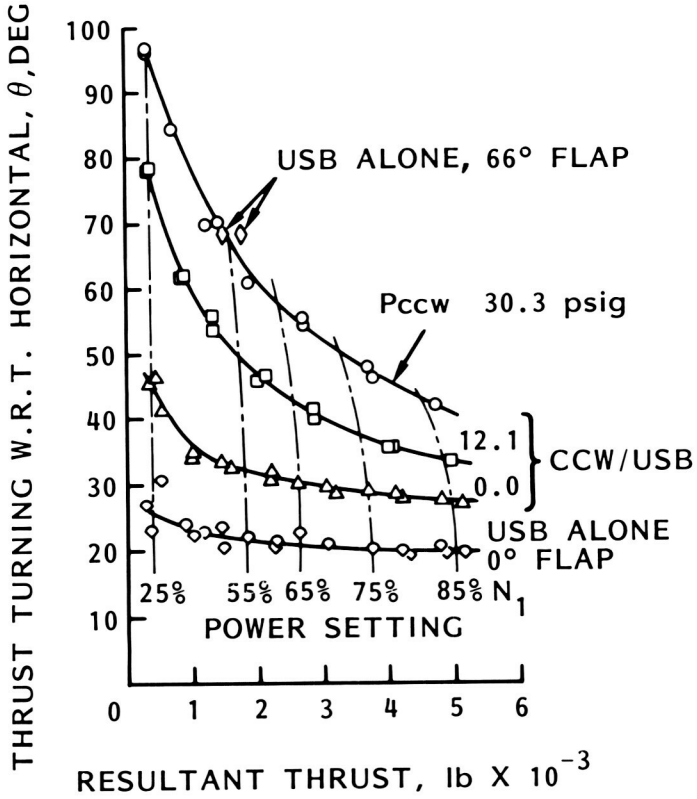

Figure 10. QSRA CCW/USB Phase I Static Thrust Turning

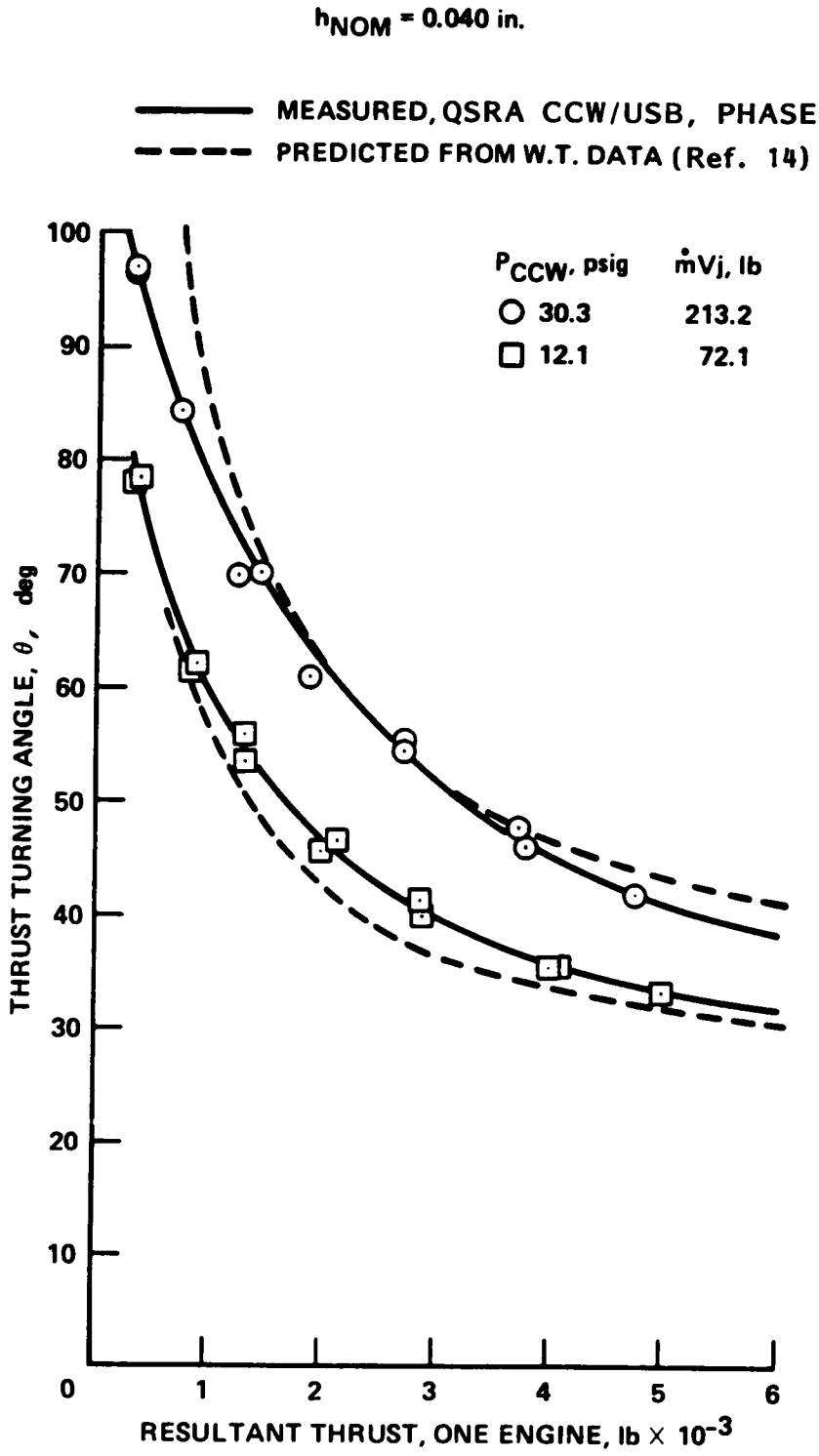

Figure 11. Phase I QSRA CCW/USB Static Thrust Turning, Predicted vs. Measured

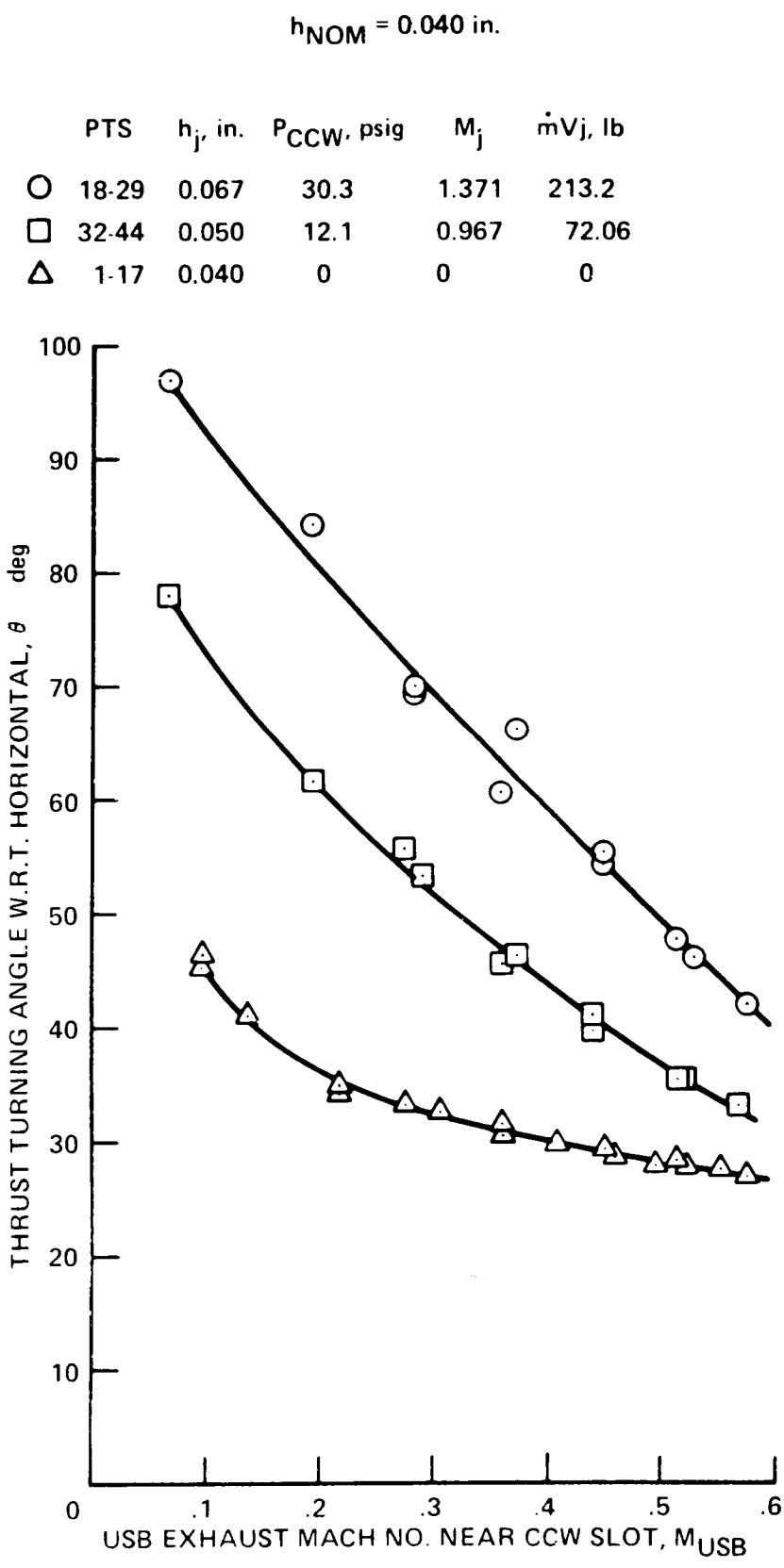

Figure 12. Phase I Static Thrust Turning as a Function of Exhaust Mach Number

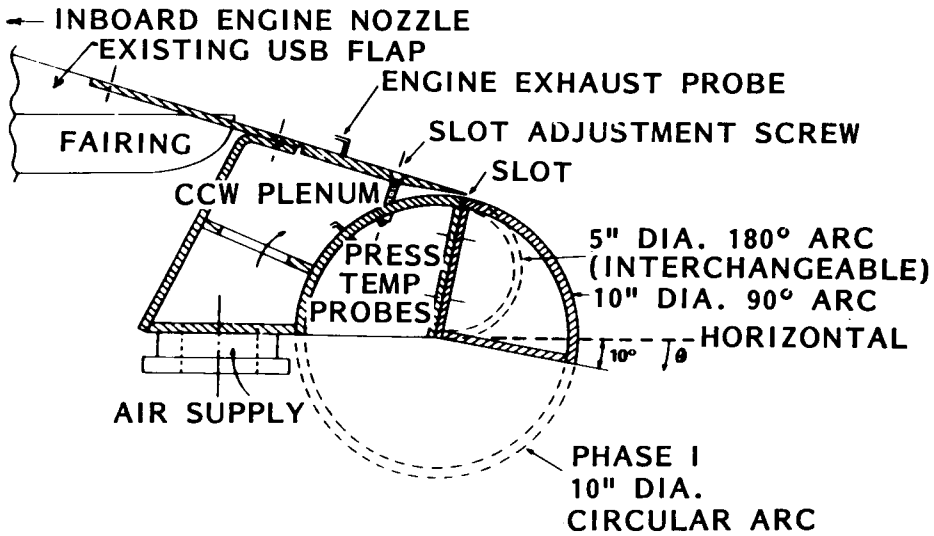

Figure 13. QSRA CCW/USB Phase II Trailing Edge Assembly

Figure 14. Ten-Inch Diameter, 90° Circular Arc Configuration

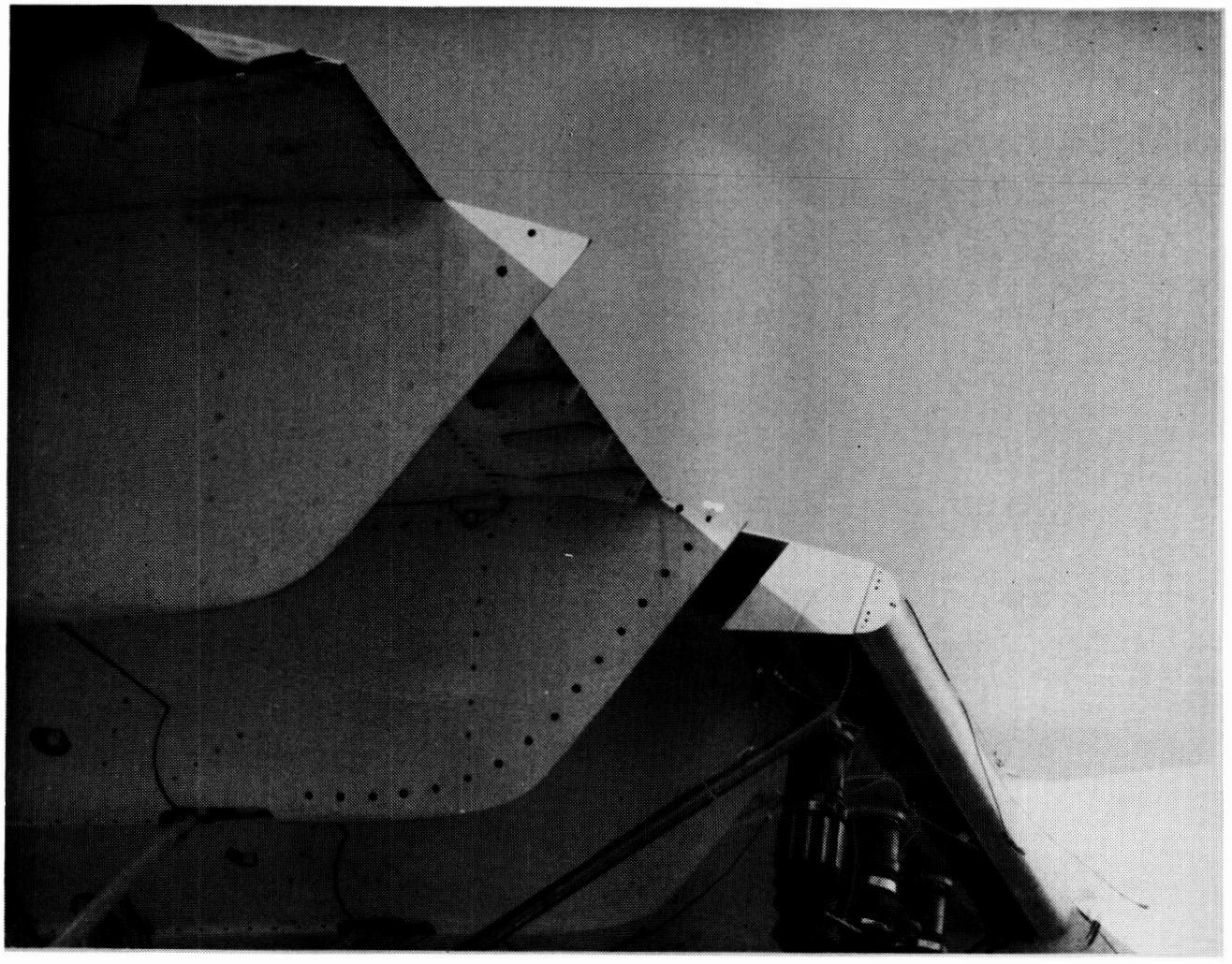

Figure 15. Five-Inch Diameter, 180^{o} Semi-Circular Configuration

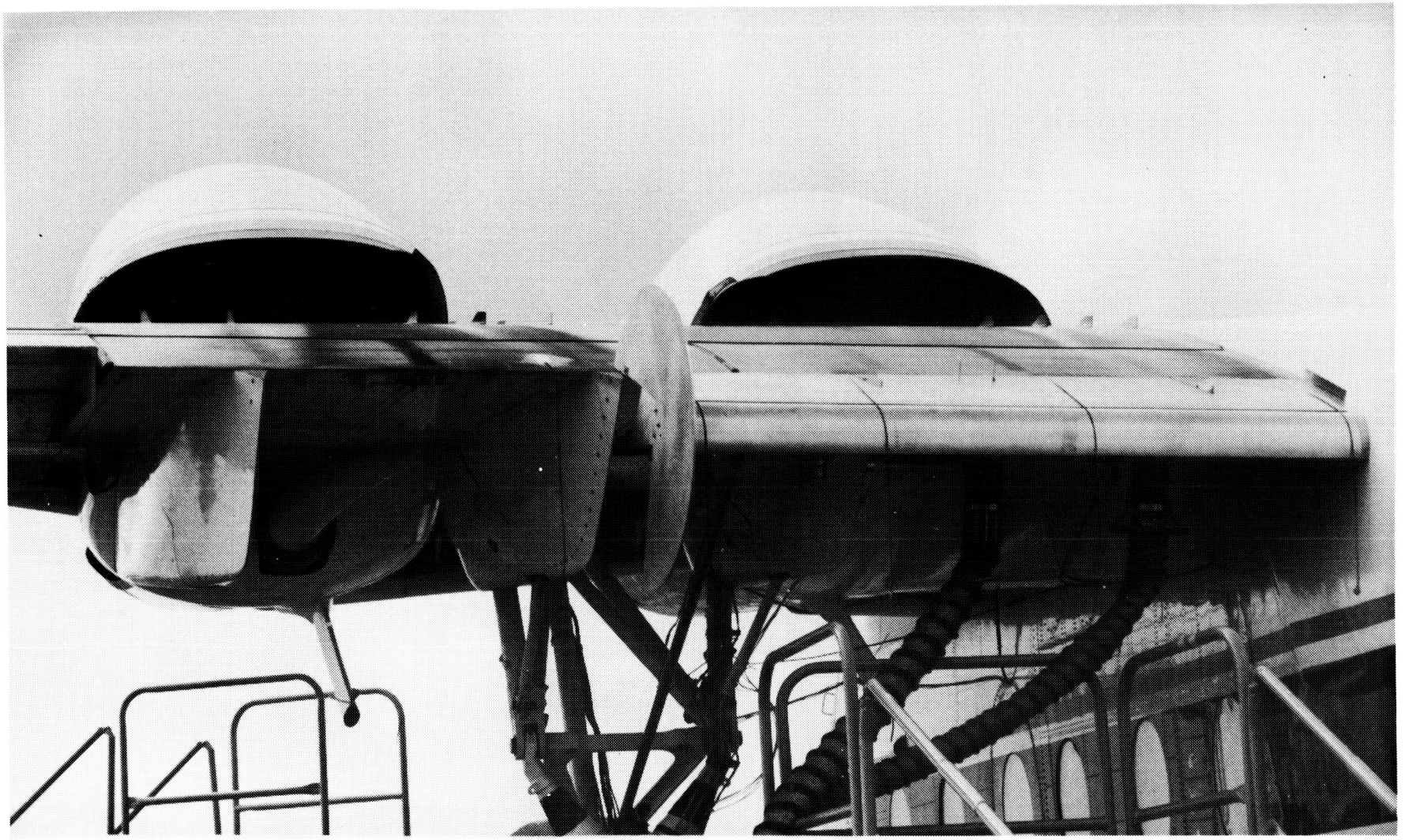

Figure 16. Flow Fence at Outboard End of Increased Span Phase II CCW Trailing Edge

Figure 17. QSRA Left Wing: CCW, Undeflected USB Flap, and Outboard Double-Slotted Mechanical Flap

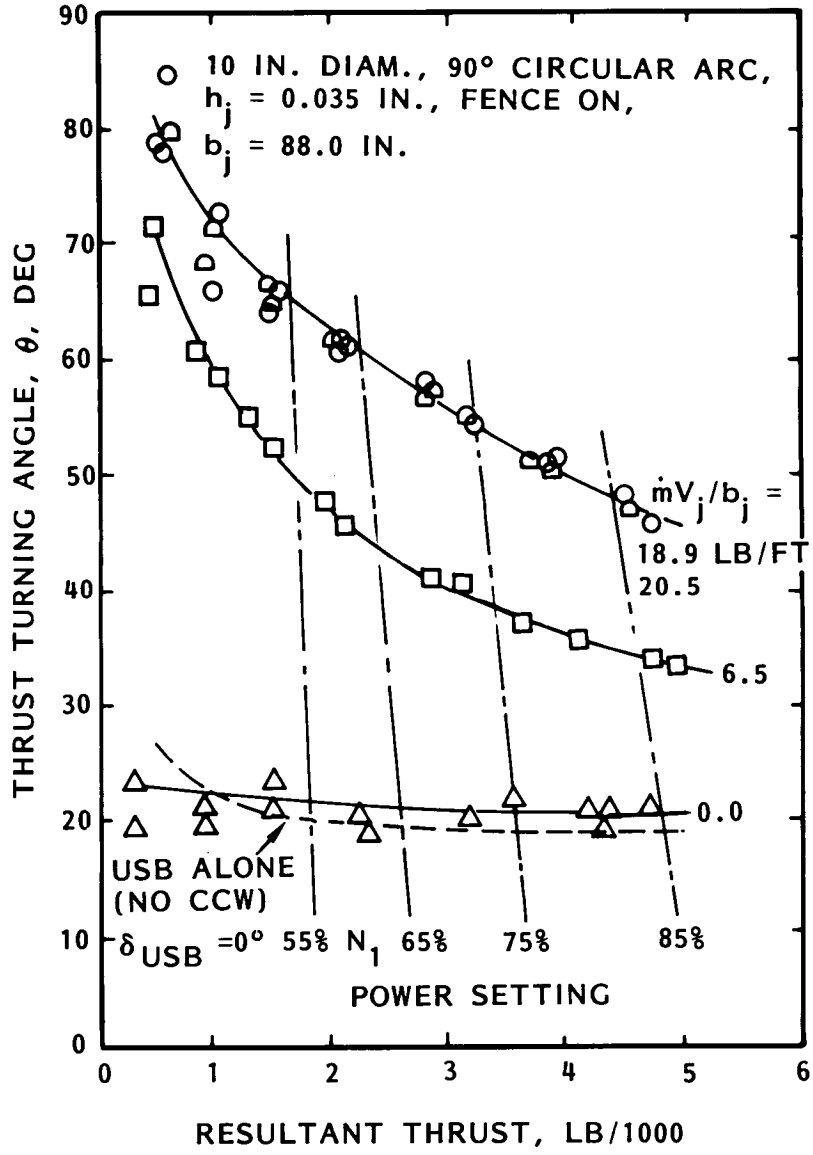

Figure 18. Phase II Static Thrust Turning for Configuration 3

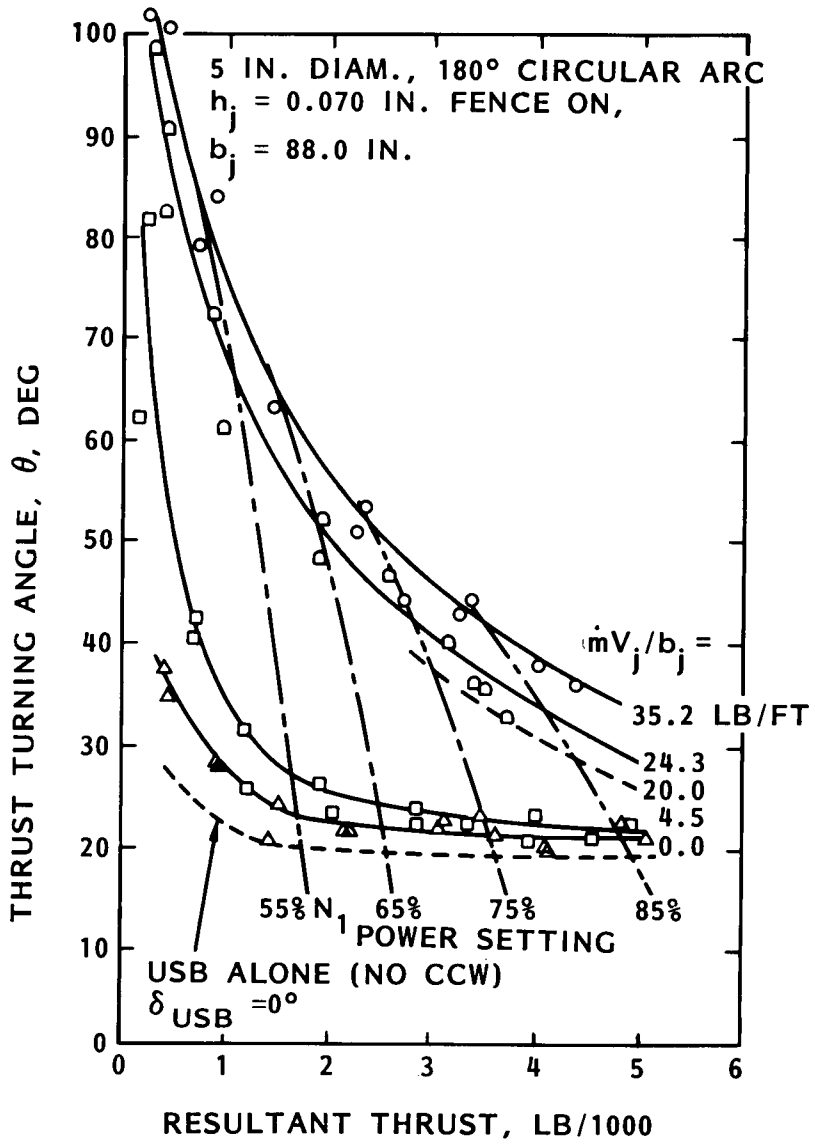

Figure 19. Phase II Static Thrust Turning for Configuration 5

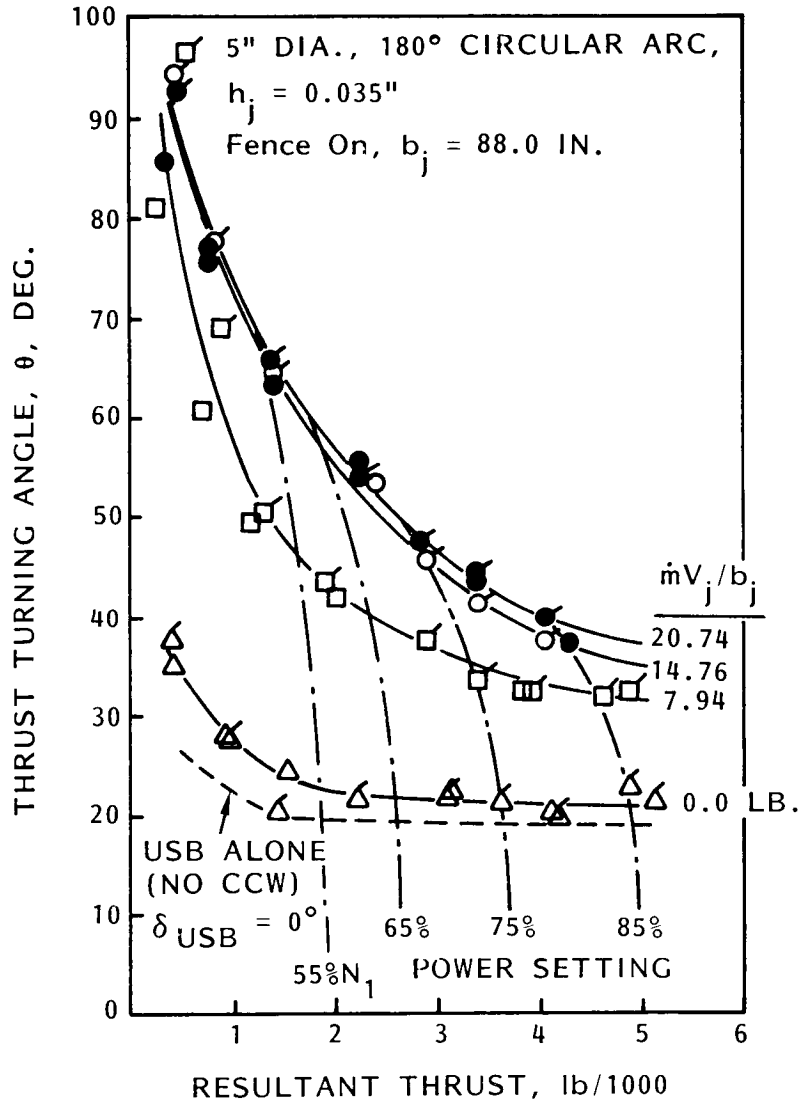

Figure 20. Phase II Static Thrust Turning for Configuration 4

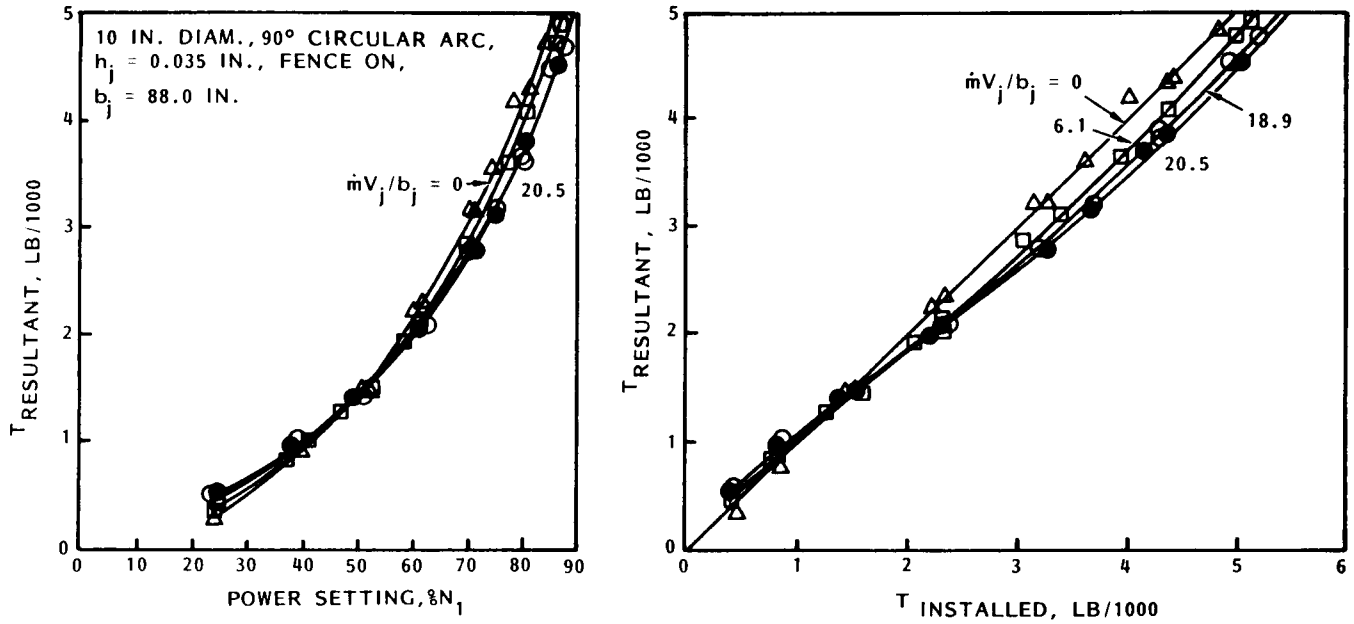

Figure 21. Effect of Blowing on Resultant Engine Thrust, Phase II, Configuration 3

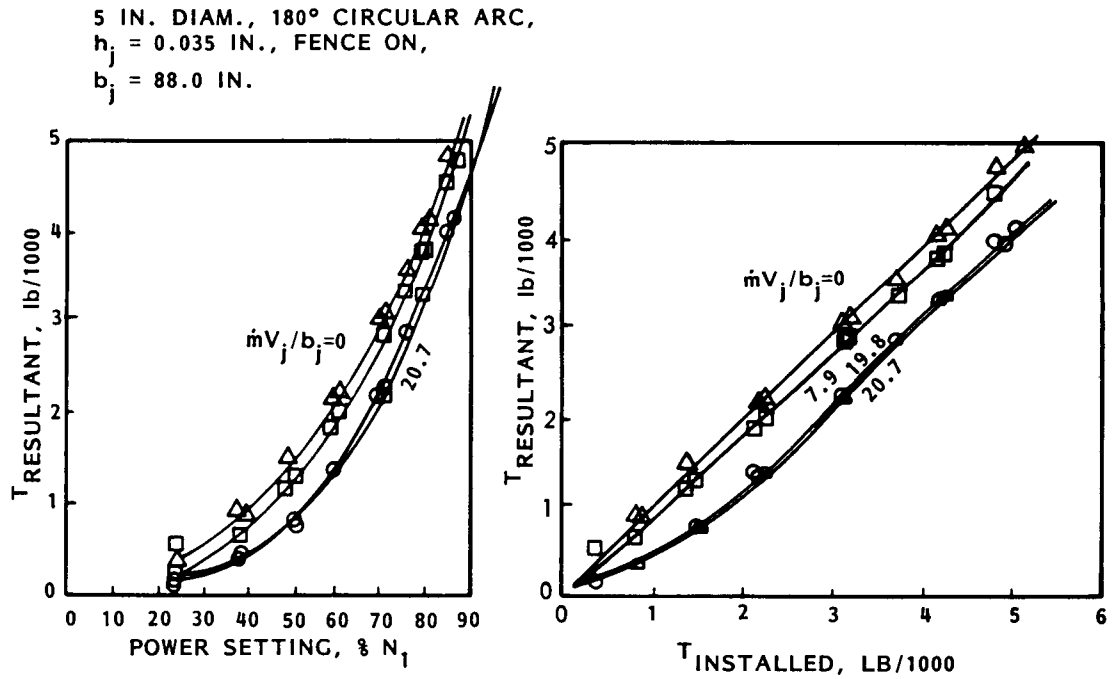

Figure 22. Effect of Blowing on Resultant Engine Thrust, Phase II, Configuration 4

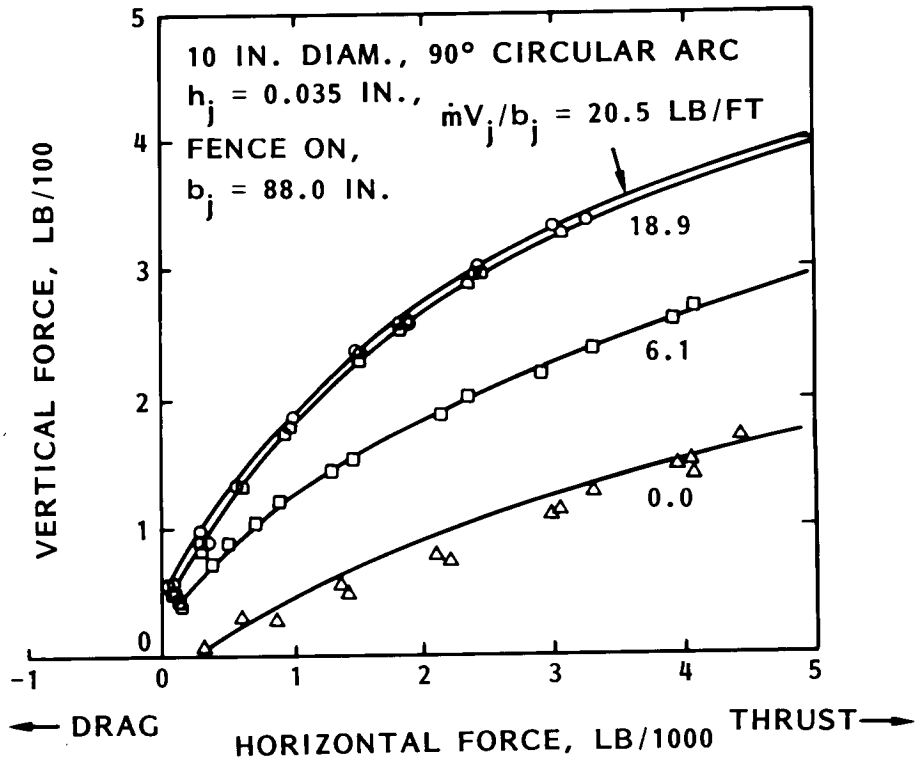

Figure 23. Static Thrust Components Due to Blowing, Phase II, Configuration 3

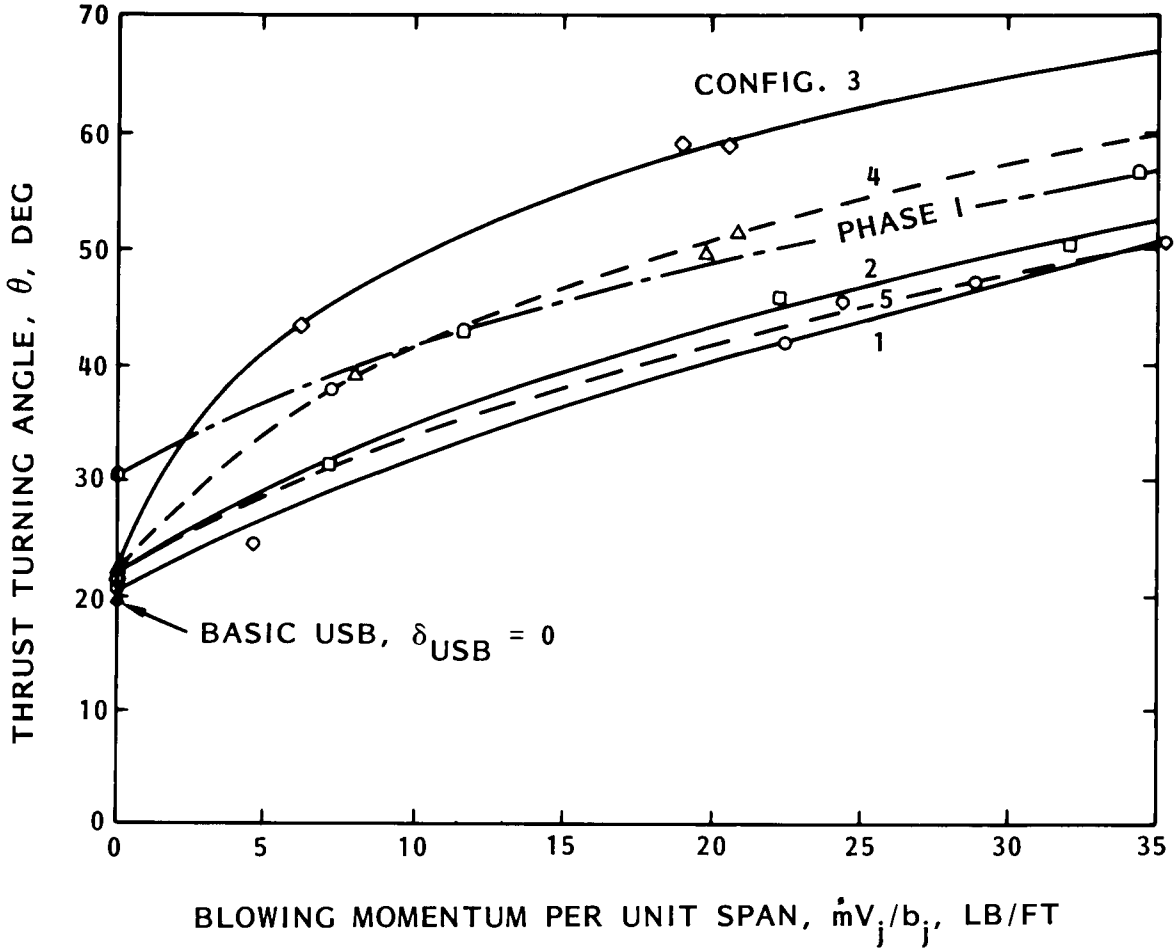

Figure 24. Comparison of Thrust-Deflecting Capability at 2500 lbs. of Resultant Thrust

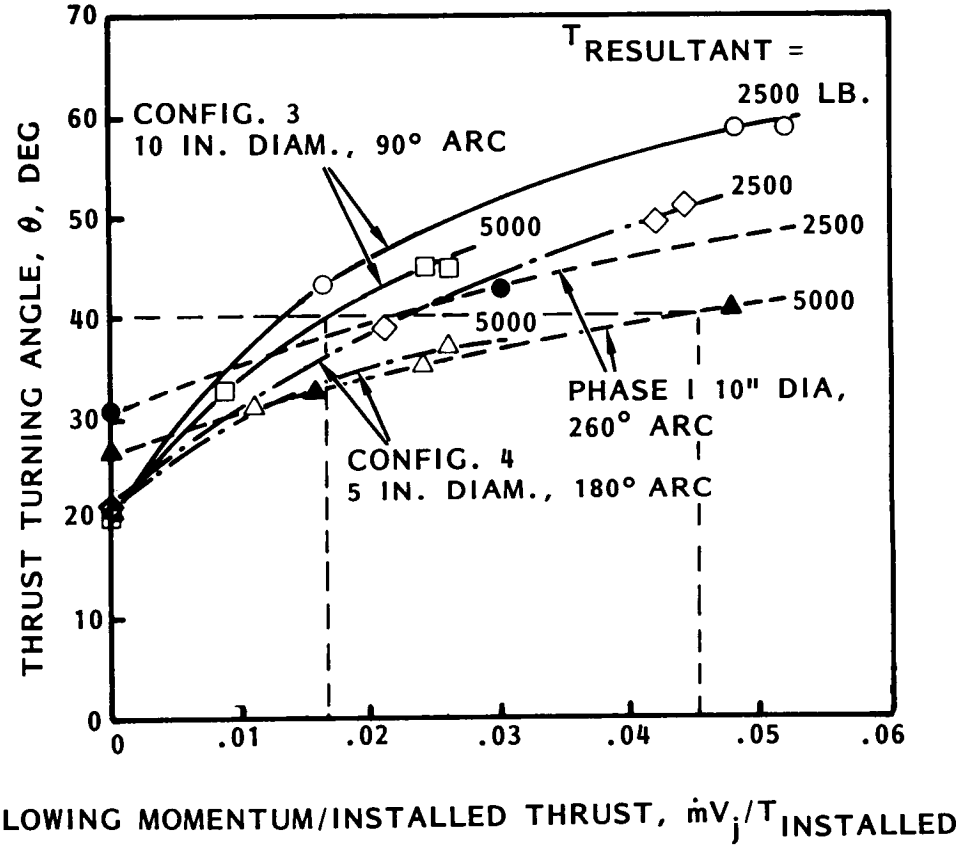

Figure 25. Comparison of CCW Blowing Momentum Required for Thrust Turning

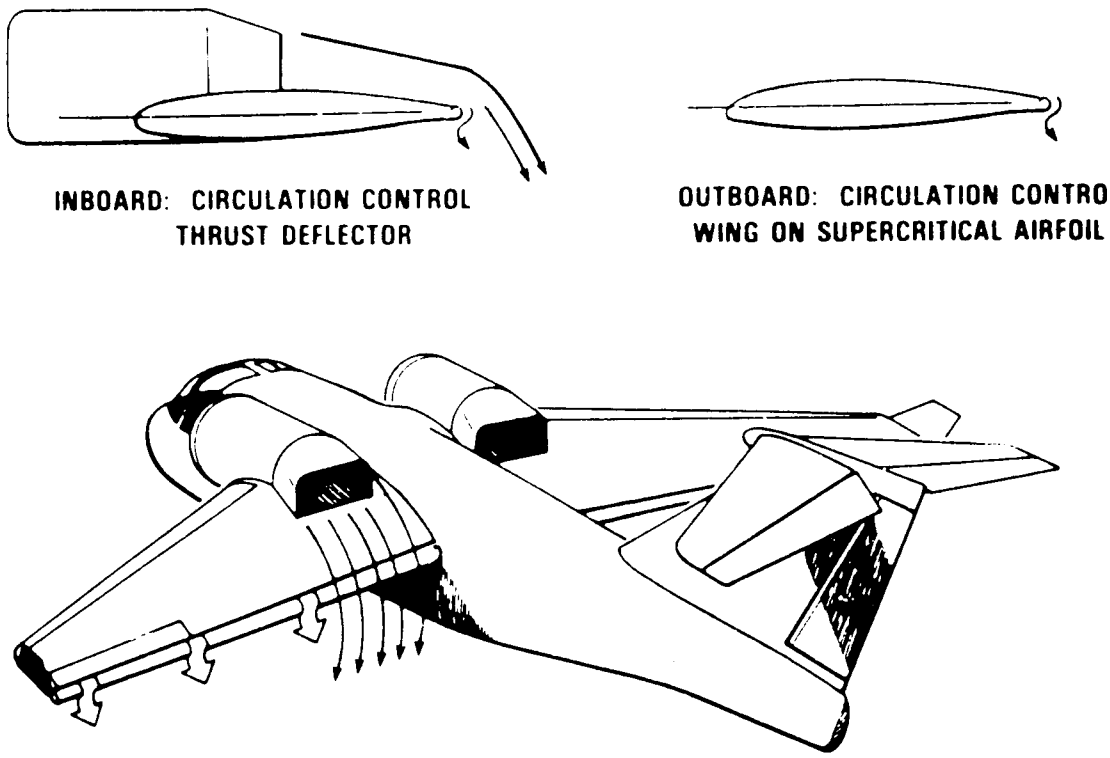

Figure 26. Proposed S-3A-Based CCW/USB STOL Aircraft

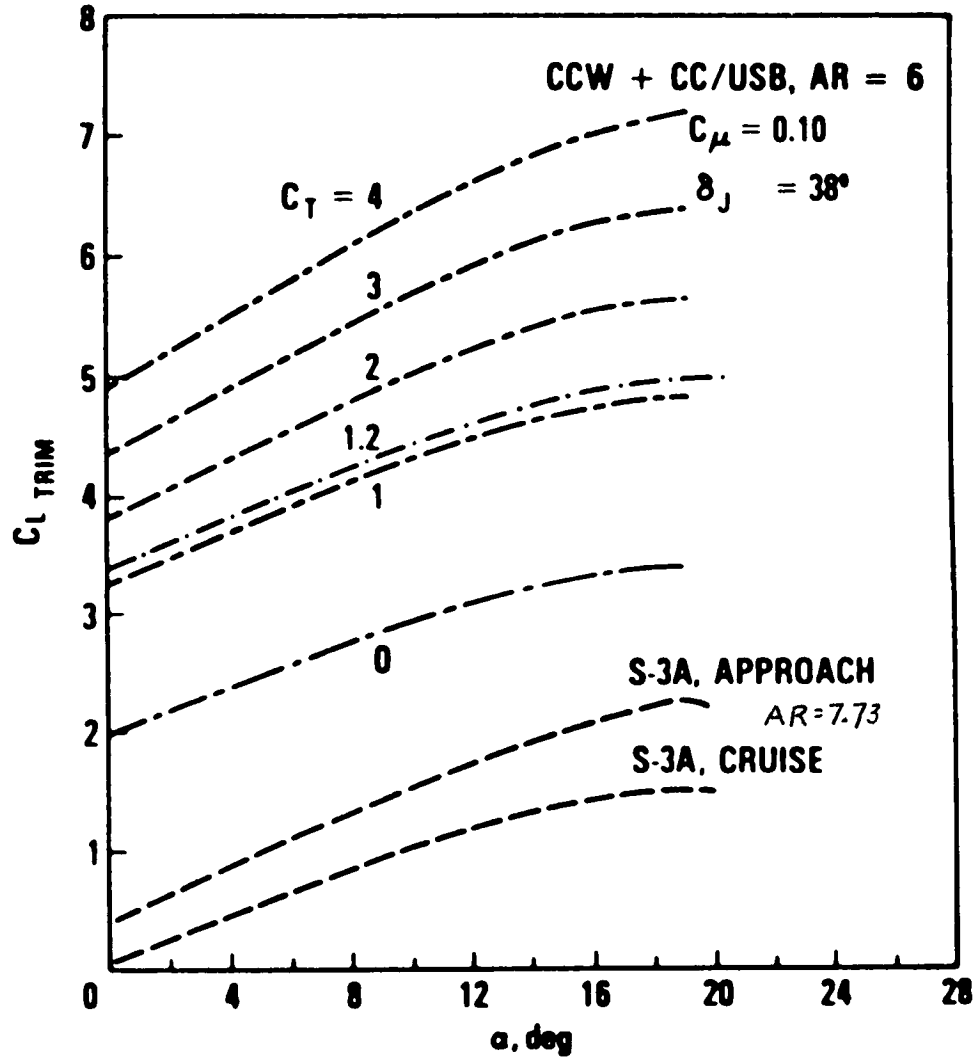

Figure 27. High-Lift Capability of Conventional S-3A and Proposed STOL Aircraft

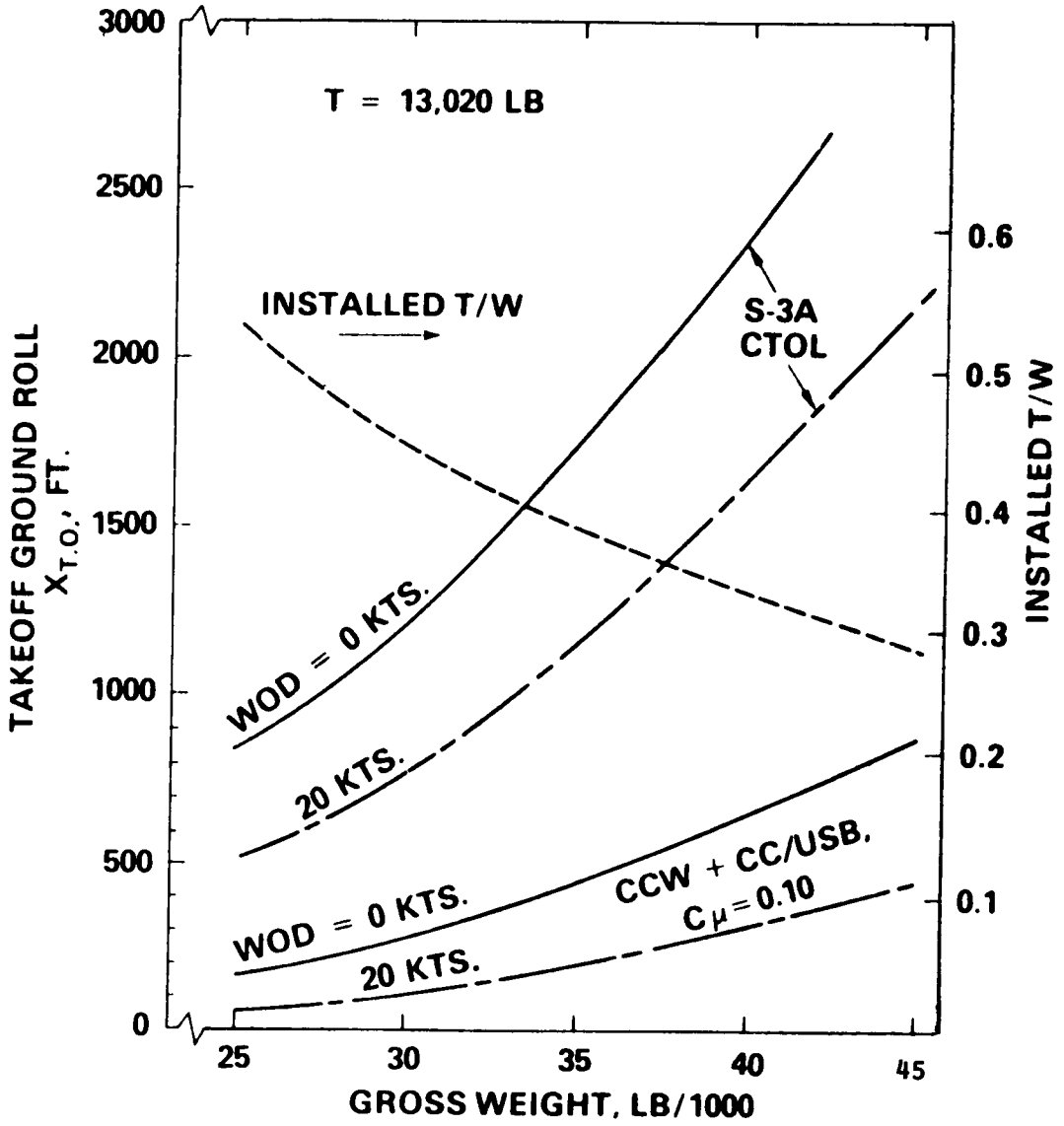

Figure 28. Comparative Unassisted Takeoff Ground Rolls on a Sea-Level Tropical Day

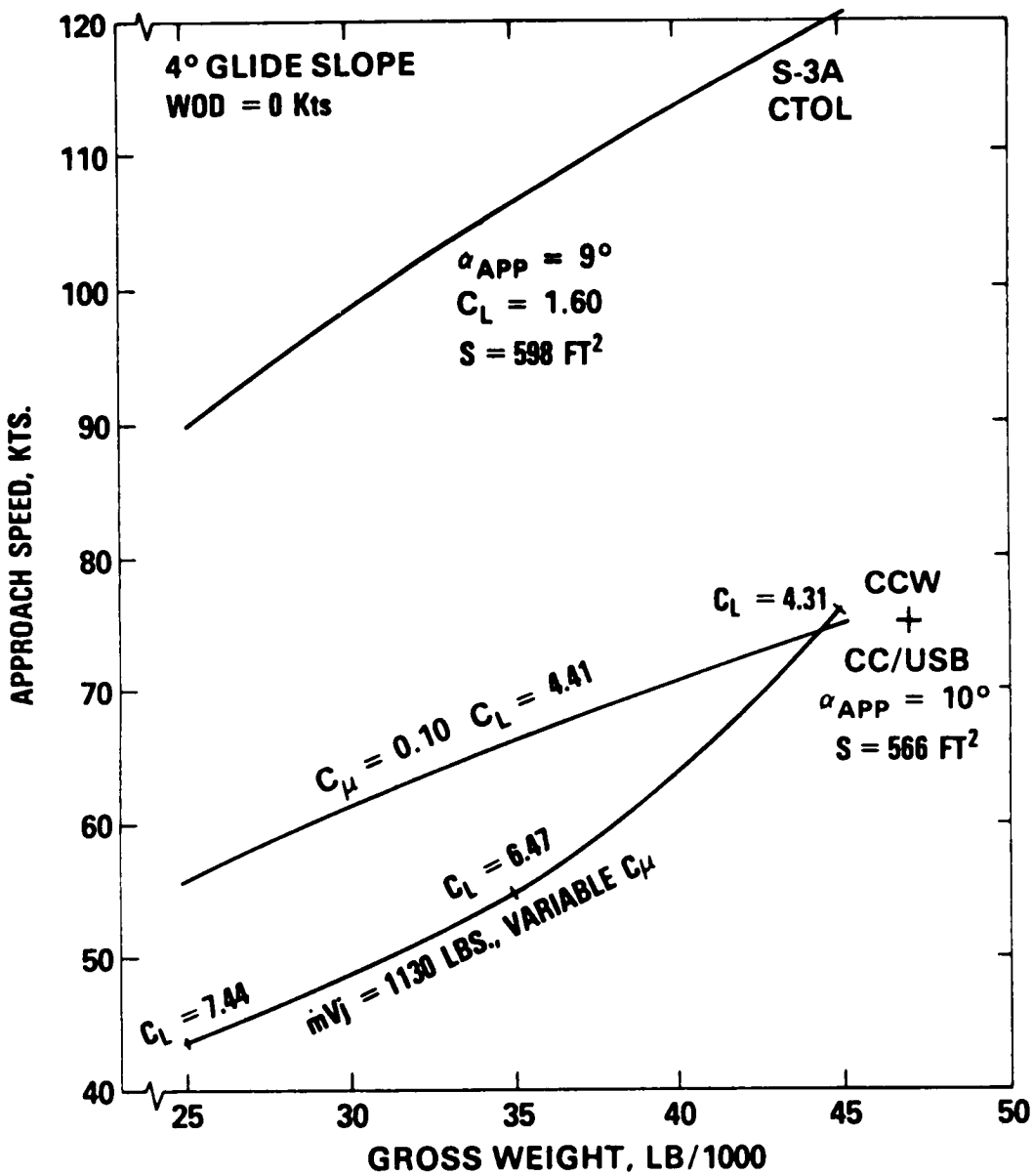

Figure 29. Equilibrium Approach Speeds on a Sea-Level Tropical Day

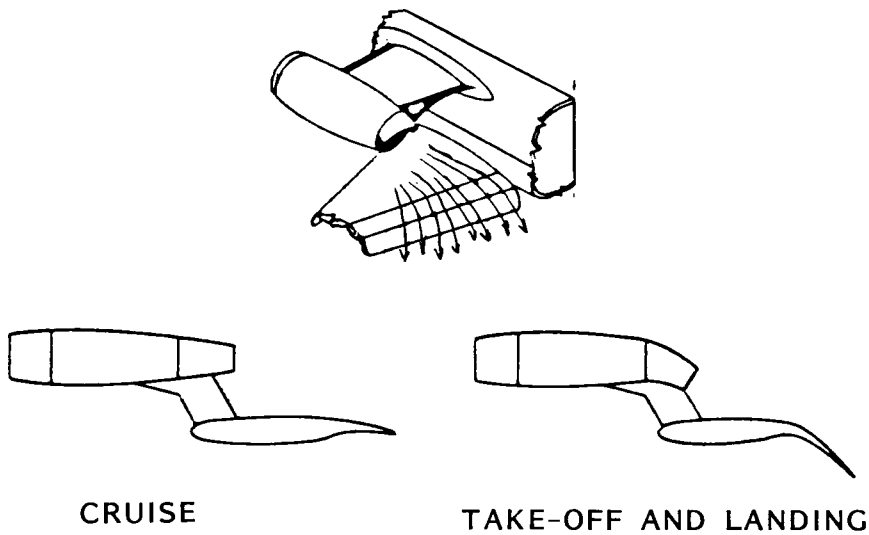

Figure 30. Over-the-Wing (OTW) Blowing Concept Using a Mechanical Flap

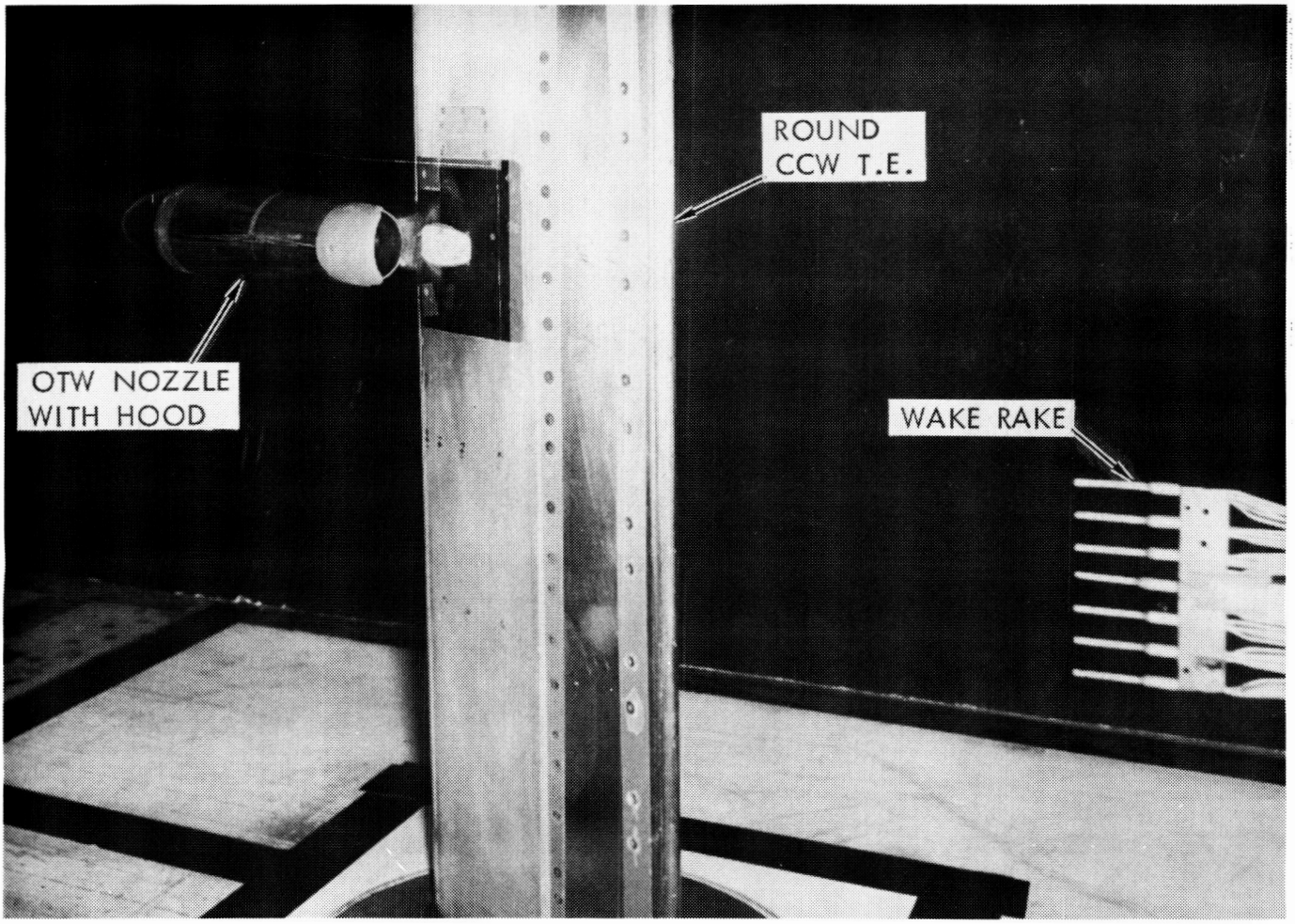

Figure 31. Quasi 2-D CCW/OTW Model in the Lockheed-GA 30-X43-Inch Model Test Facility

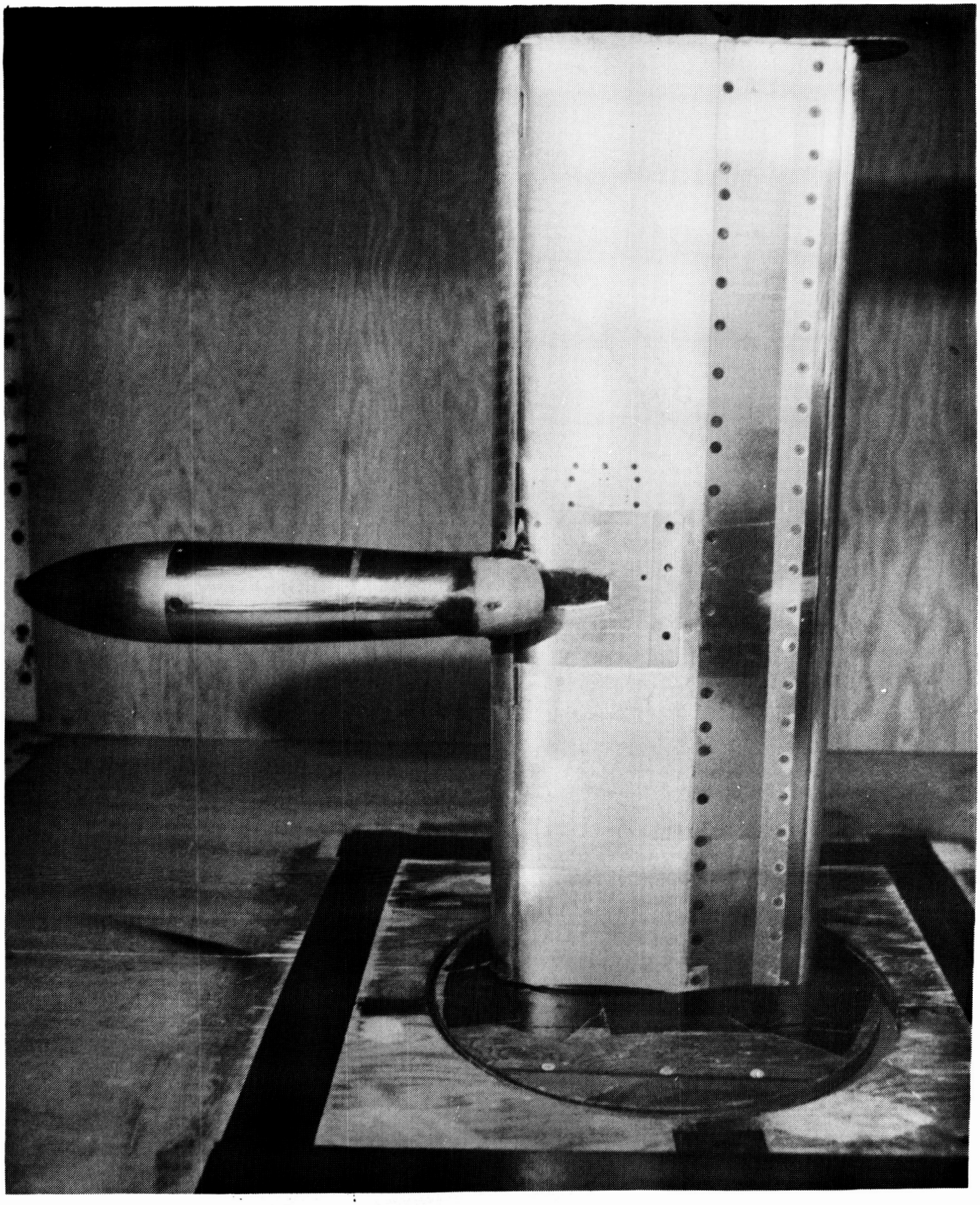

Figure 32. Semi-Span CCW/OTW Aspect-Ratio = 5.5 Model

ORIGINAL PAGE IS
OF POOR QUALITY

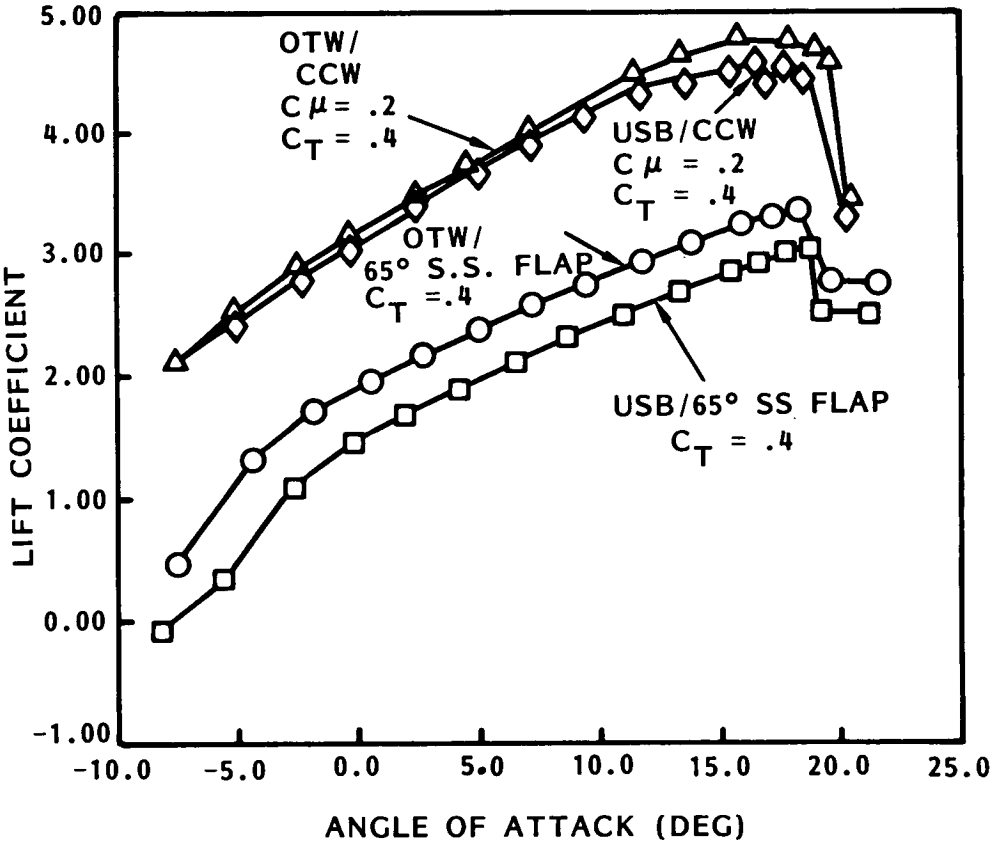

Figure 33. Quasi 2-D Comparison of CCW and Mechanical Flaps on OTW and USB Configurations

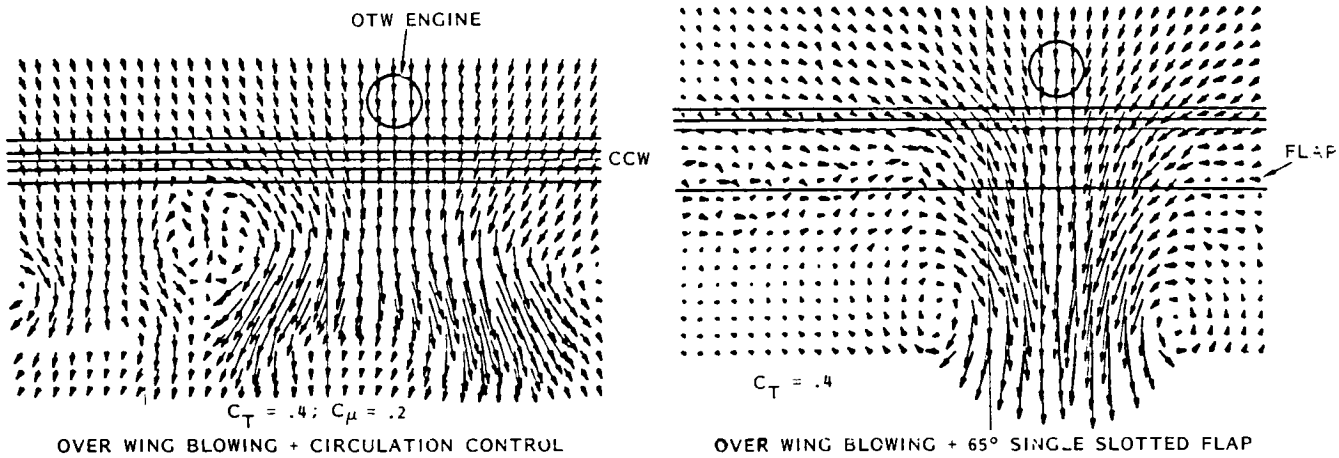

Figure 34. Wake Surveys Comparing the Effect of Trailing Edge Type with OTW Engine Arrangement

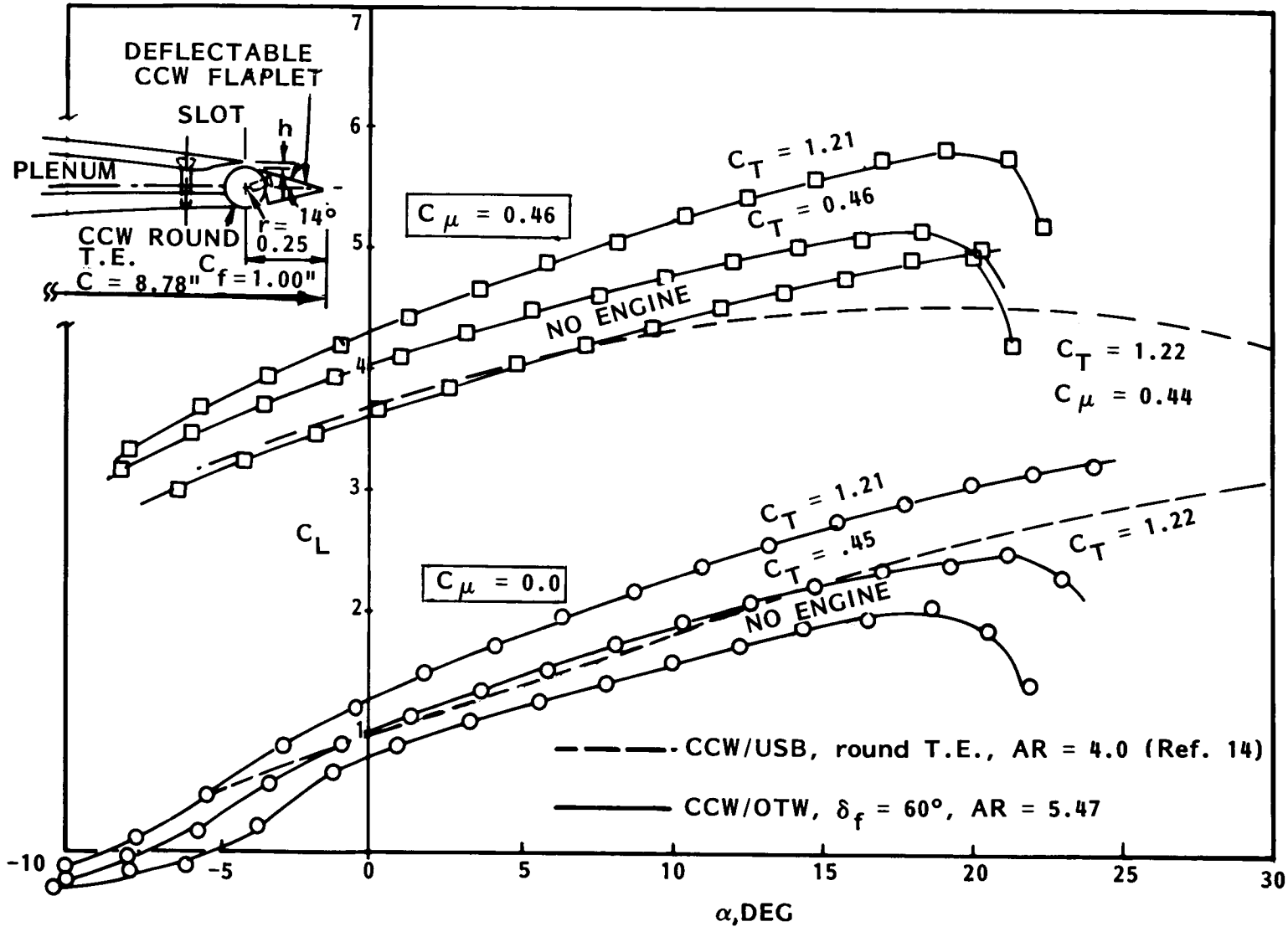

Figure 35. CCW/OTW Semi-Span Model Lift due to Blowing and Thrust Deflection, $\delta_F = 60^o$

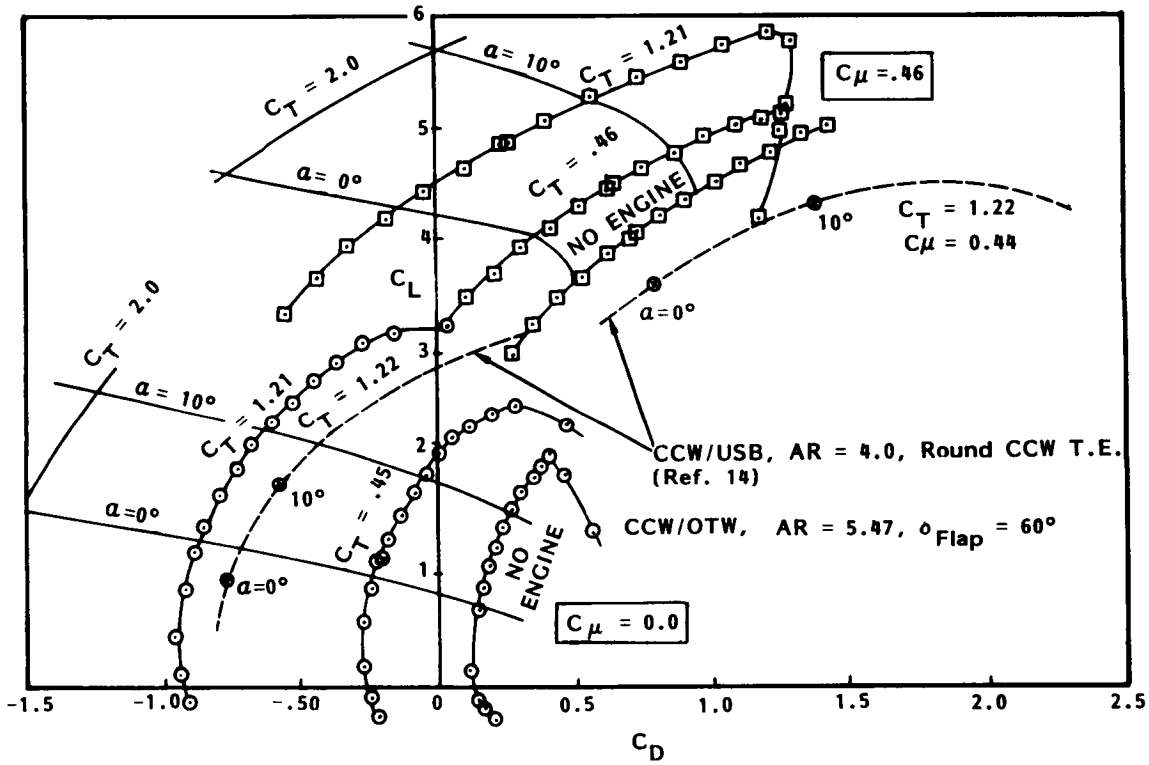

Figure 36. Comparative Drag Polars for CCW/OTW and CCW/USB Semi-Span Models

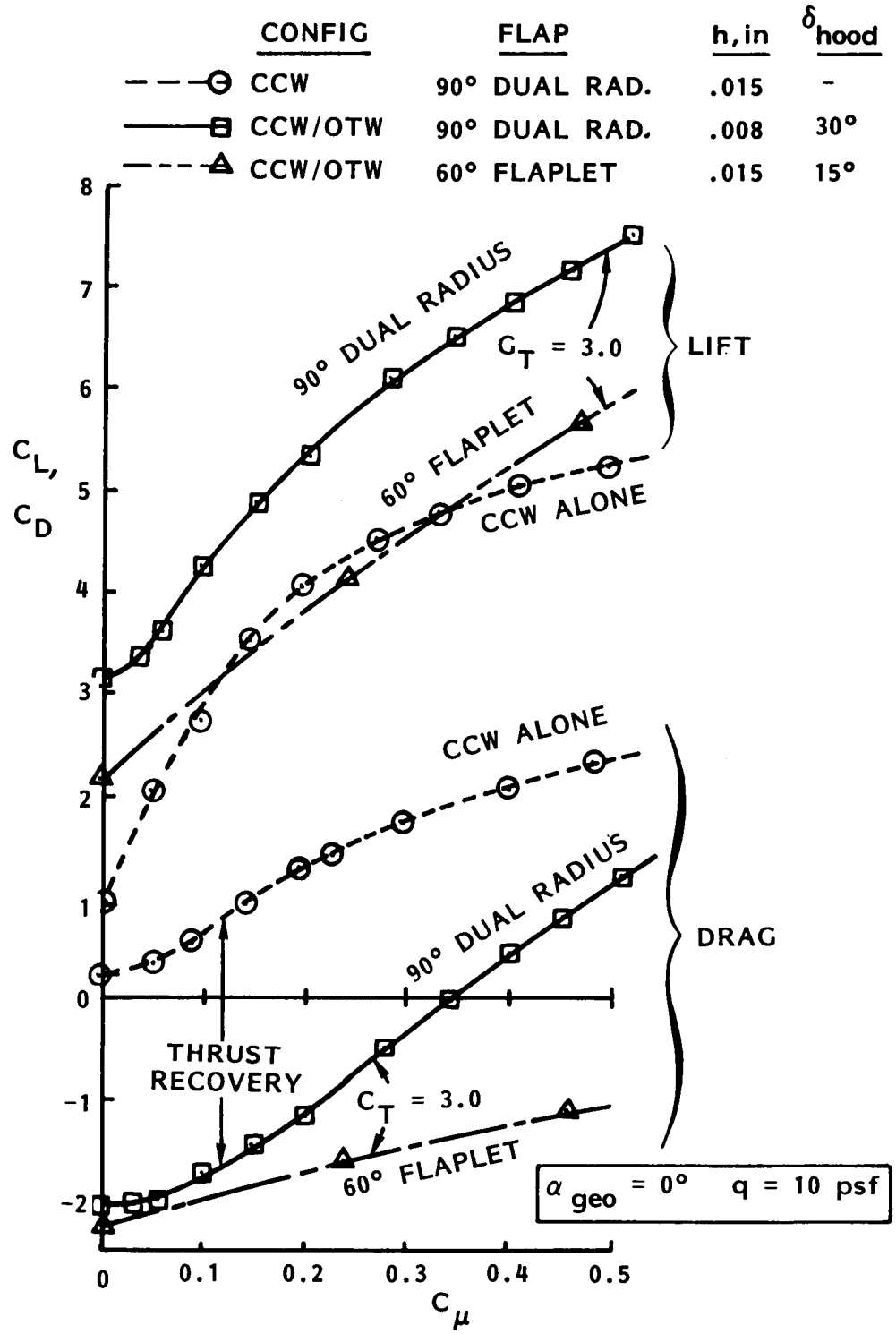

Figure 37. Effect of CCW Configuration on Lift and Drag due to Blowing and Thrust Deflection